Identification of MARVELlous Protein Markers for *Phytophthora infestans* Extracellular Vesicles

Susan Breen[1]*, Hazel McLellan[1]*, Wei Wang[1]*, Shumei Wang[1], Lydia Welsh[2], Jasmine Pham[1,3], Stephen C Whisson[2], Petra C Boevink[2§], & Paul RJ Birch[1,2§].

[1] Division of Plant Sciences, School of Life Science, University of Dundee (at James Hutton Institute), Invergowrie, Dundee DD2 5DA, United Kingdom; [2] Department of Cell and Molecular Sciences, James Hutton Institute, Invergowrie, Dundee DD2 5DA, United Kingdom; [3] Molecular Cell and Developmental Biology, School of Life Sciences, University of Dundee, Dundee DD1 4HN.

* These authors contributed equally to this work and are ordered alphabetically

§ Authors for correspondence: P.Birch@dundee.ac.uk; Petra.Boevink@hutton.ac.uk.

Abstract

Extracellular vesicles (EVs) are released from cells by unconventional secretion, but little is known about the biogenesis routes, composition or cargoes of EVs from fungal or oomycete plant pathogens. We investigated the proteome of EV-associated proteins secreted by the oomycete *Phytophthora infestans*, cause of potato late blight disease. We found that vesicle-associated proteins, transmembrane proteins and RxLR effectors, which are delivered into host cells to suppress immunity, were enriched in the EV proteome. By contrast, the EV-independent secreted proteome was enriched in cell wall modifying enzymes and apoplastic effectors which act outside plant cells. Two proteins each containing two tetraspanning MARVEL domains, PiMDP1 and PiMDP2, were associated with *P. infestans* EVs. PiMDP1 and PiMDP2 were co-buoyant with RxLR effectors in sucrose density fractions containing EVs and co-localised frequently with each other and with RxLRs at vesicles within pathogen hyphae grown *in vitro* and during infection. Interestingly, PiMDP2, which is up-regulated during the early biotrophic phase of infection, accumulates at the haustorial interface, a major site of effector secretion during infection. We argue that PiMDP1 and PiMDP2 are molecular markers that will facilitate studies of the biogenesis and secretion of infection-associated *P. infestans* EVs.

Keywords

Phytophthora infestans, extracellular vesicles, RxLR, MARVEL domain, pathogen effector

1. INTRODUCTION

Phytophthora infestans is an economically important oomycete plant pathogen. It is the causal agent of late blight disease of potato and tomato and was responsible for the Irish potato famines in the mid-1800s (Kamoun et al. 2015). It is still relevant today, causing devastating crop loses and requiring the use of expensive and environmentally unfriendly chemical sprays (Tiwari et al. 2021). To protect food security, it is crucial to understand the mechanisms by which *P. infestans* causes disease.

An important infection strategy of *P. infestans* is its ability to produce virulence factors called effectors which are usually small proteins secreted by the pathogen. These can be apoplastic effectors, which are conventionally secreted and act in the extracellular space to inhibit host enzymes, degrade substrates or mask the presence of pathogen associated molecular patterns (PAMPs) (Wang et al. 2017; 2018; Sabbadin et al. 2021); or they can be cytoplasmic effectors which act inside host cells to manipulate and interfere with plant defences (Wang et al. 2023c). The most important class of cytoplasmic effectors in *P. infestans* contain the conserved motif Arg-any amino acid-Leu-Arg (RxLR), which are encoded by more than 500 genes in the *P. infestans* genome (Haas et al. 2009). The RxLR motif is required for effector translocation into living plant cells (Whisson et al. 2007). RxLR effectors have been reported to be non-conventionally secreted from pathogen haustoria (Wang et al. 2017; 2018). Cytoplasmic effectors from the fungal pathogen *Magnaporthe oryzae* are also exported by an unconventional secretion pathway (Giraldo and Valent 2013). Furthermore, cytoplasmic effectors from both *M. oryzae* and *P. infestans* have both been demonstrated to enter plant cells via Clathrin-mediated endocytosis after being observed in vesicle-like compartments in the pathogens' specialised secretory structures (Oliveira-Garcia et al. 2023; Wang et al. 2023b).

Extracellular vesicles (EVs) are small lipid bilayer nanoparticles naturally released by cells in a form of non-conventional secretion. EVs have been extensively studied in mammalian systems

58 and exist in several different forms; including exosomes released during the fusion of
59 multivesicular bodies with the plasma membrane (PM); microvesicles produced directly from
60 the PM; and autophagosomes released from cells undergoing apoptosis (Cai et al. 2021). EVs
61 are involved in cell-to-cell communication within organisms but are also implicated in
62 interactions between organisms and could play an important role during plant pathogen
63 interactions, as demonstrated recently in the interaction between model plant *Arabidopsis*
64 and fungal pathogen *Botrytis cinerea* (He et al. 2023; Wang et al. 2024).

65 To study EVs, it is crucial to identify marker proteins to enable the purification and
66 identification of sub-populations of EVs; as well as to allow investigation of biogenesis
67 pathways. In mammalian and plant systems tetraspanin proteins, which have four
68 transmembrane (TM) domains and are integral membrane proteins, have been extensively
69 used for this purpose. Plants have several different subtypes of EVs, including those associated
70 with the markers TET8 or PEN1, which can be differentially purified using these membrane
71 proteins (Cai et al. 2018; Rutter and Innes 2017; Cai et al. 2021). However, tetraspanin
72 orthologues have not been identified in all EVs, including those from many fungi, so other
73 membrane marker proteins such as SUR7 have been proposed (Dawson et al. 2020). SUR7 is
74 a four TM containing protein normally located to MCC1/eisosomes in fungi. Eisosomes are
75 stable membrane invaginations which serve as specific membrane microdomains thought to
76 be enriched in membrane transport and endocytosis (Lanze et al. 2020). SUR7 was found to
77 be enriched in EVs from *Candida albicans* and the fungal pathogen of plants, *Zymoseptoria*
78 *tritici* (Dawson et al. 2020; Hill and Solomon 2020).

79 Little is known about EVs from oomycete plant pathogens. One study has indicated that
80 tetraspanins produced by oomycetes may act as PAMPs in plant hosts (Zhu et al. 2023) and
81 another showed that applying EVs to leaf tissue during infection can promote pathogenicity
82 (Fang et al. 2021). Here, ultracentrifugation-mediated EV purification and liquid
83 chromatography-mass spectrometry were used to determine an EV-associated proteome
84 resulting in the identification of MARVEL domain-containing TM proteins as candidate EV
85 membrane marker proteins. The MARVEL-containing markers are co-buoyant in sucrose
86 density fractions with RxLR effectors and co-localise with them at vesicles in the pathogen
87 both *in vitro* and during infection. These findings can be subsequently used by the community
88 to investigate the roles of EVs in pathogenicity in *P. infestans*.

89

90 ## 2. MATERIALS AND METHODS

91 ### 2.1 *Phytophthora infestans* growth, plant growth and plant inoculation

92 *Phytophthora infestans* strain 3928A and transgenic lines made from this strain were cultured
93 on Rye Agar (Welsh and Whisson 2025) supplemented with Ampicillin (100 µg/ml) and
94 Pimaricin (0.001 %). Geneticin (10 µg/ml) was added to select for and maintain transgenic
95 lines. *Nicotiana benthamiana* and *Solanum tuberosum* susceptible cultivar Maris Piper were
96 grown in glasshouses in a 16/8-hour light-dark cycle. Plant leaves were inoculated on the
97 abaxial surface with 10 µl drops of sporangia solution obtained by flooding a plate of 14 day
98 old culture with sterile distilled water (SDW), scraping with a glass spreader and filtering
99 through a 70 µm cell strainer into a 50 ml falcon tube. Sporangia solutions were centrifuged
100 at 2700 rpm for 10 minutes and pellets were resuspended in fresh SDW, counted on a cell
101 counter and adjusted to a concentration of 1000 sporangia per 10 µl drops.

102 ### 2.2 Endo-vesicle Isolation from *P. infestans*

103 Endo-vesicles were isolated using 1–2 g of mycelia homogenized in an equal volume of
104 isolation buffer (150 mM Na-HEPES, pH 7.5, 10 mM EDTA, 10 mM EGTA, 17.5% [w/w] sucrose,
105 7.5 mM KCl, 10 mM DTT, 1× PIC-W, 1× PIC-D, and 1× E-64) (Reynolds et al. 2014; Wang et al.
106 2023b). Cellular debris was removed by centrifugation at 2,000 × g for 20 minutes at 4 °C. The
107 resulting supernatant was transferred into pre-chilled 1.5 mL Eppendorf tubes. The
108 supernatant was divided into two equal volumes. One portion was treated with Triton X-100
109 to a final concentration of 1%, while the other received an equal volume of isolation buffer.
110 Both samples were incubated on ice for 30 minutes with gentle shaking twice during
111 incubation. Following this, they were ultracentrifuged at 100,000 × g for 60 minutes. The
112 resulting pellets were resuspended in 2× SDS loading buffer for subsequent
113 immunoblotting.**2.3 EV Isolation**

114 14-day old Rye agar plates were flooded with 20 ml of amended lima bean (ALB) liquid media
115 supplemented with the appropriate antibiotics scraped with a glass spreader into a sterile
116 culture bottle through a 70 µm cell strainer and grown for 3 days in the dark without shaking.
117 Mycelia were transferred into fresh culture bottles containing 15 ml minimal media and 15 ml
118 ALB which had been pre-cleared by ultracentrifugation at 100 000 × g for 2.5 hours. Cultures

119 were grown for a further 2 days. The culture filtrate (CF) was obtained by removing the mycelia
120 with a 70 µm cell strainer. The CF was centrifuged for 10 minutes at 2000 × g, filtered through
121 a 0.45 µm syringe filter, followed by a further spin at 10,000 × g for 30 minutes to remove all
122 cellular debris. The CF was then ultracentrifuged at 100,000 × g for 1 hour at 4 ^{o}C (Beckman
123 Coulter Type50.2 Ti rotor) to give the supernatant (100S) and crude pellet (100P) samples.

124 **2.4 Transmission Electron Microscopy (TEM)**

125 A 25 µl aliquot of EV 100P sample was mixed with 25 µl of 4% paraformaldehyde (PFA) in 0.1
126 M sodium phosphate pH 7.4 to give a final concentration of 2% PFA. 25 µl of this was pipetted
127 onto a piece of parafilm and a carbon-coated, formvar, 300 mesh, nickel grid was placed on
128 top and incubated at room temperature for 30 minutes. Grids were washed with 1 X PBS twice
129 then incubated for 10 minutes with 50 µl 1% glutaraldehyde. Grids were washed with 100 µl
130 sterile water seven times and stained with 4% uranyl oxalate for 10 minutes at room
131 temperature. Grids were transferred onto two 50 µl drops of uranyl acetate (0.15%
132 methylcellulose and 0.4% uranyl acetate) sequentially and left on the second drop for 10
133 minutes on ice. Excess liquid was wicked off using filter paper and grids were inspected and
134 imaged with a JEOL 1400, at 80 kV.

135 **2.5 Nanoparticle Tracking (NTA)**

136 Particle size and concentration of EV pellet fractions was determined using a NanoSight light
137 microscope NT10 with a 638 nm red laser or a NanoSite NS300 with a 488nm blue laser
138 (Malvern Instruments). EV pellet samples were diluted between 1:4 to 1:6 with 1x PBS, filter
139 sterilised using a 0.22 µM syringe filter (Millipore). NanoSight NTA 2.3 or NanoSite NTA3.4
140 software was used with settings of camera level 7-10, detection threshold 8-11, at room
141 temperature with 3 to 5 replicate 30 second or 1-minute reads to collect data.

142 **2.6 FM4-64 staining**

143 Pellet samples were mixed 1:1 with FM4-64 for a final dye concentration of 20 µg/ml and
144 imaged on microscope slides with the 561nm laser on a Nikon A1R confocal microscope using
145 a x60 Nikon CFI Plan Apochromat VC WI water immersion lens with an NA of 1.2. Emissions
146 were collected at 570-620 nm and the pinhole was set to 1 airy unit NIS-Elements or ImageJ
147 were used to process the images.

148 **2.7 Proteomics Sample Processing**

149 Samples were four independent biological replicates of each of the *P. infestans* culture filtrate
150 EV pellet and the supernatant from the 100,000 × g ultracentrifugation spin. Four independent
151 biological replicates of pellets and 100,000 × g supernatants from media-only control spins,
152 not containing *P. infestans*, were also used and treated in the same way. For the supernatant
153 samples 2 ml of each was subjected to methanol-chloroform precipitation and pellets were
154 air dried. All samples were resuspended in 50 µl 0.25% Rapigest™ SF (Waters) in 50 mM
155 ammonium bicarbonate. Protein concentration was determined by taking 2.5 µl of each
156 sample and carrying out a scaled down version of the BCA assay (Pierce) according to
157 manufacturer's instructions. DTT was added to the remaining sample to a final concentration
158 of 5 mM and samples were boiled at 100 ^{o}C for 5 minutes. Samples were passed to the
159 'FingerPrints' Proteomics Facility, School of Life Sciences, University of Dundee where they
160 were subsequently processed. Samples were alkylated by adding 1.5 µl (500 mM
161 Iodoacetamide) and incubated for 30 min the dark at RT. Digestion was achieved by adding 56
162 µl of ammonium bicarbonate containing 7.5 µg of trypsin/sample and incubation at 37 ^{o}C for
163 14 hrs. Peptides were acidified with TFA (0.5% final concentration) and incubated at 37 ^{o}C for
164 60 min to precipitate Rapigest. Samples were finally centrifuged at 13,000 rpm for 10 min, and
165 supernatant containing peptides were transferred to new vials. Samples were resuspended in
166 50 µl 1 % formic acid and stored at -22 ^{o}C prior to LC-MS analysis.

167 **2.8 LC-MS/MS**

168 Analysis of peptide readout was performed on a Q Exactive™ plus, Mass Spectrometer
169 (Thermo Scientific) coupled to a Dionex Ultimate 3000 RS (Thermo Scientific). LC buffers used
170 were the following: buffer A (0.1 % formic acid in Milli-Q water (v/v)) and buffer B (80 %
171 acetonitrile and 0.1 % formic acid in Milli-Q water (v/v). An equivalent of 1.25 µg of peptides
172 from each sample were loaded at 10 µl/min onto a trap column (100 µm × 2 cm, PepMap
173 nanoViper C18 column, 5 µm, 100 Å, Thermo Scientific) equilibrated in 0.1 % TFA for 15min.
174 The trapping column was washed for 6 min at the same flow rate with 0.1 % TFA and then
175 switched in-line with a Pharma Fluidics, 200 cm, µPAC nanoLC C18 column, equilibrated with
176 buffer A at a flow rate of 300 nl/min for 30 min. The peptides were eluted from the column at
177 a constant flow rate of 300 nl/min with a linear gradient from 1 % buffer B to 3.8 % buffer B in

178 6 min, from 3.8 % B to 12.5 % buffer B in 40 min, from 12.5 % buffer B to 41.3 % buffer B within
179 176 min and then from 41.3 % buffer B to 61.3 % buffer B in 34 min. The gradient was finally
180 increased from 61.3 % buffer B to 100 % buffer B in 10 min, and the column was washed at
181 100 % buffer B for 10 min. Two blanks were run between each sample to reduce carry-over.
182 The column was kept at a constant temperature of 50 ^{o}C. Q-exactive plus was operated in
183 positive ionization mode using an easy spray source. The source voltage was set to 2.2 Kv and
184 the capillary temperature was 275 ^{o}C. Data were acquired in Data Independent Acquisition
185 (DIA) Mode as previously described (Doellinger et al. 2020), with little modification. A scan
186 cycle comprised a full MS scan (m/z range from 345-1155), resolution was set to 70,000, AGC
187 target 3×10^6, maximum injection time 200 ms. MS survey scans were followed by DIA scans
188 of dynamic window widths with an overlap of 0.5 Th. DIA spectra were recorded at a
189 resolution of 17,500 at 200 m/z using an automatic gain control target of 3×10^6, a maximum
190 injection time of 55 ms and a first fixed mass of 200 m/z. Normalised collision energy was set
191 to 25 % with a default charge state set at 3. Data for both MS scan and MS/MS DIA scan events
192 were acquired in profile mode.

193 **2.9 Proteomics Data Analysis**

194 Analysis of the DIA data was carried out using Spectronaut (version 17.4.230317.55965,
195 Biognosys, AG). The directDIA workflow, using the default settings (BGS Factory Settings) with
196 the following modifications was followed: decoy generation set to mutated; Protein LFQ
197 Method was set to QUANT 2.0 (SN Standard) and Precursor Filtering set to Identified (Qvalue);
198 Cross-Run Normalization was unchecked; Precursor Qvalue Cutoff and Protein Qvalue Cutoff
199 (experimental) were set to 0.01; Precursor PEP Cutoff set to 0.1 and Protein PEP Cutoff set to
200 0.75; Protein Qvalue Cutoff (Run) set to 0.05. For the Pulsar search, the settings were:
201 maximum 2 missed trypsin cleavages; PSM, Protein and Peptide FDR levels set to 0.01;
202 scanning range set to 300-1800 m/z and Relative Intensity (Minimum) set to 5%; cysteine
203 carbamidomethylation set as fixed modification and acetyl (N-term), deamidation
204 (asparagine, glutamine), dioxidiation (methionine, tryptophan), glutamine to pyro-Glu and
205 oxidation of methionine set as variable modifications. Separate searches were made against
206 the fasta files for *Phytophthora infestans* (strain T30-4; UP000006643, 17,610 entries) and
207 *Phaseolus vulgaris* (UP000000226; 30,501 entries). Analysis of differential protein abundance
208 for the *P. infestans* data was carried out in Excel with the Spectronaut output. Peptides that

209 appeared to represent *P. infestans* proteins were removed if they were also identified in
210 greater than 3 out of the 8 media control samples as an additional control for
211 misidentification. Positive protein identification was confirmed only if there were >1 peptide
212 identified over 3 out of 4 biological replicates. Perseus version 2.0.6.0
213 (http://www.coxdocs.org/doku.php?id=perseus:start) was subsequently used to do PCA
214 analysis and produce volcano plot (2- sided t-test with 250 randomisations with a permutation
215 based FDR calculation, FDR= 0.05, S0= 0.1). If proteins were not detected in either P or S
216 samples they were given a value of zero in those samples to include them in the volcano plot.

217 **2.10 Construction of *P. infestans* transgenic lines**

218 The vector pmCitrine:mCherry used to co-express proteins of interest tagged with mCitrine
219 and mCherry each under the control of the *Bremia lactucae* Ham34 promotor (Ham34P) and
220 terminator (Ham34T) was based on pMCherryN (Ah-Fong and Judelson 2011) with the
221 mCitrine cassette cloned into the Sac I site. Coding sequences of Pi04314 (XM_002905913.1),
222 Pi09216 (XM_002903466.1), Pi13660 (XM_002899798.1), Pi13661 (XM_002899799.1), PiPE1
223 (XM_002909508.1), PiGNB2L (XM_002903143.1), PiRab7 (XM_002906189.1), PiCoronin
224 (XM_002908188.1) and PiAVRblb1 (XM_002895005.1), were amplified from *P. infestans*
225 isolate 3928A cDNA with the primers shown in Supplementary Table S1 and were cloned as
226 either C or N terminal protein fusions to the fluorescent proteins using restriction enzyme
227 cloning and standard molecular biology techniques. Plasmids were sequenced to confirm the
228 correct inserts and Plasmid prepped using the Promega PureYield™ Plasmid Maxiprep System.
229 Transformation of *P. infestans* isolate 3928A was performed using a modified polyethylene
230 glycol-$CaCl_2$-lipofectin protocol (Judelson et al. 1991; Welsh and Whisson 2025). Previously
231 published transformants were also used for PiEPIC1 (Wang et al. 2017), PiManl (Ah-Fong and
232 Judelson 2011), PiAvr3a (Whisson et al. 2007) and PiSCR74 (Lin et al. 2020).

233 **2.11 Triton X-100 Treatments**

234 Prior to the 100, 000 xg ultracentrifugation the CF was split into two equal volumes, one was
235 treated with Triton X-100 detergent at a final concentration of 1%, while the other had the
236 same volume of SDW added. The tubes were mixed and incubated on ice for one hour before
237 ultracentrifuging at 100, 000 × g for one hour (Beckman Coulter, Type50.2 Ti rotor). Pellets

238 were resuspended in equal volumes of 2 ×SDS protein loading buffer and equal volumes were
239 loaded on SDS PAGE gels.

240 **2.12 Sucrose Density Gradients**

241 The crude pellet from the 100,000 × g ultracentrifugation was resuspended into 1 ml 1x PBS
242 and adjusted to make a 10% sucrose solution which was top loaded onto a sucrose gradient
243 composed of 10, 20, 30, 40, 50, 60 and 70% sucrose solutions of 1.6 ml each, made up with
244 1x PBS plus Protease inhibitor tablet. Samples were ultracentrifuged for 16 hours at 4 ^{o}C at
245 100,000 xg with no brake (Beckman Coulter, SW41 rotor). Six fractions of 1.8 ml each were
246 taken, the percentage of sucrose measured using a portable refractometer (MRC, REF108 0-
247 80 % Brix, 1 %) and used to calculate sucrose density. The tubes containing the fractions were
248 topped up with 1 x PBS and then ultracentrifuged at 100,000 × g for 1 hour at 4 ^{o}C (Beckman
249 Coulter, Type50.2 Ti rotor). The resulting pellets were resuspended in either 40 μl of 1 × PBS
250 for TEM or 2xSDS PAGE loading buffer for Western blotting.

251 **2.13 Western blotting**

252 Samples were run on 10% SDS PAGE gels to separate samples and blotted onto Nitrocellulose
253 membranes. Membranes were blocked in 4 % milk in 1 x PBST (0.05 % Tween 20) for one hour
254 at room temperature. Primary antibodies for RFP/ mCherry (Chromotek, 58F) and GFP/
255 mCitrine (Roche, 11814460001) were incubated overnight at 4 °C in blocking buffer at a
256 dilution of 1:4000 or 1:2000 respectively. Membranes were washed five times in 1 × PBST and
257 the secondary antibodies IRDye® 680RD Goat anti-Rat IgG, IRDye® 800CW Goat anti-Rat IgG,
258 IRDye® 800CW Goat anti-Mouse IgG or IRDye® 680RD Goat anti-Mouse IgG (LICORbio) were
259 added. The membranes were incubated for 1 hr at room temperature in the dark in blocking
260 buffer at a dilution of 1:5000. Blots were developed on a LiCOR ODYSSEY® DLx and quantified
261 using LICOR Image Studio™ Software.

262 **2.14 Phylogenetic analysis**

263 Candidate MDP orthologs were identified by reciprocal best blast match (RBBM). Multiple
264 sequence alignment was undertaken in Clustal omega and phylogenetic trees were generated
265 using Phylogeny.fr (http://www.phylogeny.fr/) (Dereeper et al. 2008). Gene orientation and
266 spacing was recorded in the genomes where both candidate MDP1 and MDP2 orthologues

267 were identified. AlphaFold2 was used to predict the structures of PiMDP1 and PiMDP2
268 (https://colab.research.google.com/github/sokrypton/ColabFold/blob/main/AlphaFold2.ipy
269 nb).

270 **2.15 qRT-PCR**

271 Gene expression of PiMDP1, PiMDP2 and the RxLR Pi04314 was monitored using an infection
272 time-course of *P. infestans* isolate 3928A on Maris Piper potato leaves. RNA was extracted
273 using a RNeasy Plant mini kit (Qiagen). Potential DNA contamination was removed using the
274 Turbo DNA-free kit (Thermo Fisher) and cDNA was synthesised using a Superscript III kit
275 (Invitrogen). qRT-PCR was carried out using Power SYBR™ Green PCR Master Mix (Thermo
276 Fisher) and the primers shown in Supplementary Table S1, on a StepOne Real-Time PCR
277 System (Applied Biosystems). Expression was normalised to the geometric mean of 3
278 housekeeping genes: ACTIN (PITG_15117; EEY63399), Casein kinase (PITG_02745; EEY64204),
279 Kelch domain repeat (PITG_09862; XM_002902372.1) using the $2^{-\Delta\Delta Ct}$ method (Lacomme et
280 al. 2003).

281 **2.16 Confocal Microscopy**

282 *P. infestans* hyphae grown in ultracentrifuged ALB media on microscope slides were imaged
283 at 2-3 dpi and leaf infections on either potato or *N. benthamiana* leaves were imaged at 3-5
284 dpi. A Nikon A1R confocal microscope was used. Samples on slides were imaged with a x60
285 Nikon CFI Plan Apochromat VC water immersion lens (NA 1.2) while infections were imaged
286 with a x40 NIR Apo DIC water dipping lens (NA 0.8). The 514 nm line from an argon laser was
287 used to excite the mCitrine with emissions collected at 520-550 nm. A 561nm laser was used
288 to excite the mCherry and emissions collected at 570-620 nm. The pinhole was set to 1 airy
289 unit for the 561 nm line. NIS-Elements or ImageJ were used to process and quantify the
290 images. Fluorescence intensity plots drawn to show (co-)localisation in vesicle-like bodies
291 were taken from single optical sections. HM /PM ratio measurements were taken by
292 measuring the mean fluorescence intensity of comparably-sized regions of interest drawn to
293 encompass the PM or HM in single optical sections from the same z series. Counts to show
294 (co-)localisation of visually detectable fluorophores in vesicles from *in vitro* grown hyphae
295 were performed manually from a minimum of 12 confocal images for each transformant and
296 expressed as a percentage of the total number of vesicles counted.

297

298

299 **3. RESULTS**

300 **3.1 *P. infestans* secretes EVs when grown *in vitro***

301 To determine whether *P. infestans* produces EVs we aimed to isolate EVs from *in vitro* cultures
302 of wildtype *P. infestans* strain 3928A using ultracentrifugation (UC) methods (Figure 1a)
303 broadly similar to those used for other filamentous plant and animal pathogens (Hill and
304 Solomon 2020; Cai et al. 2021). Following UC, our crude pellets were resuspended and
305 examined by Nanoparticle tracking analysis (NTA) and transmission electron microscopy
306 (TEM) to verify the presence of EVs. NTA analysis showed that each of the pellets recovered
307 by UC of *P. infestans* culture media contained an average equivalent particle concentration of
308 49.13 E8 particles/ml, with an average mean diameter of 202 nm and an average mode
309 diameter of 100 nm, whereas the pellets derived from media without *P. infestans* lacked
310 particles of a similar size or concentration but contained a low level of background particulate
311 matter from the growth media (Figure 1b). TEM negative stain imaging showed the presence
312 of typical cup-shaped vesicle structures of various sizes in the *P. infestans* culture media crude
313 pellets (Figure 1c, Supplementary Figure S1a-b), whereas no vesicles were observed in the
314 pellets of media-only samples generated using the same UC method (Supplementary Figure
315 S1c). Staining of the *P. infestans* culture media crude pellet samples with lipophilic dye FM4-
316 64 indicated that theys contain membrane-bound nanoparticles (Supplementary Figure S1d),
317 whereas the uninoculated media-only pellets showed no FM4-64 staining (Supplementary
318 Figure S1e).

319 **3.2 Proteomics identifies an enrichment of EV-associated proteins**

320 Confident that we were indeed obtaining EVs isolated from *P. infestans,* we proceeded to
321 analyse the proteome of four independent replicates of the crude EV pellets and compared
322 them to the proteins precipitated from the supernatants after the EVs had been removed by
323 ultracentrifugation. The samples were all treated with Rapigest detergent to maximise
324 recovery of integral membrane proteins possessing transmembrane (TM) domains. This
325 approach yielded a starting point of 1908 proteins (Supplementary Table S2a). Low confidence

326 proteins only represented by a single peptide and *P. infestans* proteins also present in more
327 than 3 out of 8 of the media-only control samples were removed. This left 1326 high
328 confidence proteins present in at least 3 out of the 4 biological replicates (Supplementary
329 Table S2b). The EV pellet contained 450 unique proteins while the supernatant had only 23
330 unique proteins and there was an overlap of an additional 853 proteins (Figure 2a). PCA
331 multiple component analysis showed that the pellet (EV-associated) and supernatant (EV-
332 independent) samples clustered in their respective groups (Supplementary Figure S2a). GO
333 term analysis of the proteins identified in the pellet samples show enrichments of proteins
334 belonging to the functional categories of Metabolic enzymes, RNA metabolism and
335 Translation, as well as Membrane traffic, Protein modifying enzymes and Transporters
336 (Supplementary Figure S2b).

337 Perseus (version 2.0.6.0) was used to generate volcano plots determining which proteins were
338 detected at significantly different amounts between the EV-associated pellet and EV-
339 independent supernatant samples. Supplementary Figure S3a shows the volcano plot
340 highlighting the different categories of proteins which were detected differentially. Group S1
341 indicates proteins that are found exclusively in the supernatant. S2 indicates proteins that are
342 found in all supernatant samples and between 1 and 3 pellet samples but are statistically
343 enriched within the supernatant. S3 indicates proteins that are found in all samples but are
344 statistically enriched within the supernatant. Group P1 indicates proteins that are found
345 exclusively in the pellet. P2 indicates proteins that are found in all pellet samples and between
346 1 and 3 supernatant samples but are statistically enriched within the pellet. P3 indicates
347 proteins that are found in all samples but are statistically enriched within the pellet. Overall,
348 1009 proteins (76%) were enriched in the pellet, 255 proteins (19%) were enriched in the
349 supernatant and 62 proteins (5%) were not significantly over-represented in either P or S
350 samples (Table 1). 34% of proteins enriched in the supernatant were found to contain a signal
351 peptide (SP), whereas only 8% of proteins enriched in the pellet had an SP (Table 1,
352 Supplementary Table S3a).

353 Interestingly, the pellet was found to be significantly enriched in RxLR effector proteins (33
354 out of 42 proteins), suggesting that these effectors are potentially often associated with EVs
355 (Figure 2b, Table 1, Supplementary Table S3b). By contrast, apoplastic effectors (7 out of 8
356 proteins) were predominantly detected in the supernatant samples showing that

357 conventionally and non-conventionally secreted proteins may have different fates. It is worth
358 noting that a number of RxLR (19) and apoplastic (9) effectors present in the original data
359 (Supplementary Table S2a) were excluded from analyses as, being small proteins, they were
360 only represented by a single peptide and were thus not included in the high confidence
361 dataset (Supplementary Table S2b). Similar to the pattern for apoplastic effectors, secreted
362 cell wall degrading enzymes (CWDEs) were predominantly detected in the supernatant (34
363 out of 46 proteins), whereas vesicle-associated proteins were predominantly enriched in the
364 pellet samples (38 out of 41 proteins) (Figure 2c, Table 1, Supplementary Table S3b). PAMPs
365 from *P. infestans* were found to be predominantly enriched in the supernatant samples (8 out
366 of 13 proteins), although a few were enriched in the pellet (4 out of 13 proteins)
367 (Supplementary Figure S3b, Table 1, Supplementary Table S3b).

368 To provide support for the observations in the proteomics dataset, transgenic *P. infestans* lines
369 expressing a subset of genes of interest, tagged with fluorescent proteins, were subjected to
370 the EV UC protocol and western blotting was used to investigate their presence in supernatant
371 (S) and pellet (P) samples. We observed the enrichment of RxLR effectors Pi09216-mCitrine,
372 Pi04314-mCherry and PiAVRblb1-mRFP in the pellet samples, whereas apoplastic effectors
373 PiEPIC1-mRFP and PiSCR74-mRFP and the CWDE PiPE1-mCitrine were enriched in supernatant
374 samples (Figure 2d-g, Supplementary Figure S3c,d). PiAVRblb1 and PiEPIC1, although only
375 represented by single peptides were included, along with apoplastic effector SCR74 which was
376 not detected in the proteome, as we had existing, well-characterised *P. infestans*
377 transformants secreting these fusion proteins (Wang et al. 2017, 2018, 2023b). The pellet-
378 to-supernatant ratio for three RxLRs vs three apoplastic effectors was quantified for multiple
379 replicate western blots using LiCOR software and further supported patterns of enrichment in
380 the proteomics data (Supplementary Figure S3e). A transformant co-expressing Pi04314-
381 mCherry and PiPE1-mCitrine verified that these proteins were differentially enriched in pellet
382 or supernatant samples, respectively (Figure 2g). *P. infestans* transformants expressing vesicle-
383 associated proteins PiGNB2L-mCitrine and mCherry-PiRab7 also supported the proteomics
384 data, whereas, although detected in the pellet, PiCoronin-mRFP was not enriched in these
385 samples (Figure 2h-j). The control Golgi marker protein PiManI (Ah-Fong and Judelson 2011)
386 was not detected in pellet or supernatant samples showing that not all proteins associated

387 with cellular membrane compartments can be secreted or associated with EV-containing
388 samples (Figure 2k).

389 **3.3 MARVEL domain proteins are candidate EV markers**

390 To identify potential EV marker proteins we sought transmembrane (TM)-containing proteins
391 enriched in the pellet proteome. Unexpectedly, we did not identify any proteins
392 corresponding to tetraspanins which are classic membrane markers of mammalian and plant
393 EVs (Cai et al. 2021). However, we did identify 81 TM domain containing proteins and 71 of
394 these (88 %) were significantly enriched in the pellet samples (Figure 3a, Table 1,
395 Supplementary Table S3b). Of particular interest were two MARVEL domain-containing
396 proteins, hereafter referred to as *P. infestans* MARVEL domain protein 1 and 2 (PiMDP1 and
397 PiMDP2). A MARVEL domain consists of a bundle of four TM helices and PiPMDP1 and PiMDP2
398 each have two MARVEL domains, so contain a total of eight TM helices (Figure 3b) with the N-
399 and C- termini predicted to be on the same side of the membrane. Interestingly yeast protein
400 non classical export (NCE102) is a MARVEL domain protein which localises with the fungal EV
401 marker SUR7 to eisosomes and is enriched in fungal EVs from *Candida albicans* (Dawson et al.
402 2020). This prompted us to examine PiMDP1 and PiMDP2 in more detail. Phylogenetic analysis
403 using reciprocal best blast hit (RBBH) matches (Supplementary Figure S4a) showed that
404 PiMDP1 and PiMDP2 candidate orthologues exist in all *Phytophthora* clades with PiMDP2 also
405 present in many *Pythium* species indicating it is likely ancestral to PiMDP1. However,
406 orthologues of these genes were not identified in the downy mildews as homology searches
407 only yielded single MARVEL proteins that were not RBBH matches. Generally, each
408 *Phytophthora* species has one copy of each *MDP* gene and these are arranged head-to-head
409 with a small intervening region of several hundred base pairs (Supplementary Figure S4b),
410 likely indicating a conserved evolutionary origin.

411 The expression of *PiMDP1* and *PiMDP2* was examined during infection of Potato leaves with
412 *P. infestans* and indicated that, while both genes are upregulated during infection (Figure 3c,
413 Supplementary Figure S5a-b) *PiMDP1* transcript levels steadily increase throughout the
414 infection time course, with the highest level at 72 hours post-inoculation (hpi). By contrast,
415 *PiMDP2* expression is higher at the earlier timepoints of 24 and 48 hpi and thus more closely
416 resembles the expression profile of RxLR effectors, such as *Pi04314,* which act as markers of

417 the biotrophic phase of infection where *P. infestans* is coexisting with living plant tissue
418 (Whisson et al. 2007).

419 To assess the suitability of PiMDP1 and PiMDP2 as candidate EV markers dual transgenic *P.*
420 *infestans* lines were made co-expressing either PiMDP1-mCitrine or PiMDP2-mCitrine with
421 RxLR effector Pi04314-mCherry. Initial EV ultracentrifugation preparations indicated that both
422 PiMDP1 (Figure 3d) and PiMDP2 (Figure 3e) accumulate in the pellet and not the supernatant
423 of the 100,000 g spin. To provide further evidence that these proteins are associated with EVs
424 the culture filtrate was equally divided and one half was treated with detergent 1% Triton X-
425 100 prior to the 100,000 x g spin. Figure 3f shows that in the presence of Triton significantly
426 less PiMDP1 is recovered as detected by western blotting and quantified using the LICOR
427 quantification system. The same result was observed with PiMDP2 (Figure 3g). TEM analysis
428 of pellets without Triton showed the presence of EV-like structures (Figure 3h) whereas in the
429 presence of Triton no EVs were observed (Figure 3i). These results suggest that these
430 candidate markers are associated with membranous EV-like structures which are sensitive to
431 disruption with detergents such as Triton. As PiMDP1 and 2 are predicted to be integral
432 membrane proteins IP experiments were carried out to determine if the termini of these
433 proteins are present within or exposed on the surface of the vesicular structures.
434 Supplementary Figure S6 shows that C-terminally tagged PiMDP1-mCitrine and PiMDP2-
435 mCitrine are only immunocaptured in the presence of the detergent triton suggesting that the
436 tagged ends are inside the EVs, and thus not exposed until vesicles are disrupted
437 (Supplementary Figure S6a-b). The same result is observed when each of the N-termini are
438 tagged with mCherry (Supplementary Figure S6c-d).

439 To further characterise these marker proteins the crude pellets of the transgenic *P. infestans*
440 lines were subjected to further separation and purification on sucrose density columns. Firstly,
441 a transformant co-expressing two RxLRs, Pi09216-mCitrine and Pi04314-mCherry (Figure 4a-
442 b, Supplementary Figure S7a-b), showed each effector fusion to accumulate predominantly in
443 Fraction 4 with a sucrose density of ~1.16 to 1.18 g/cm^2. MARVEL marker candidate PiMDP1-
444 mCitrine and RxLR Pi04314-mCherry were observed also to predominantly co-accumulate in
445 sucrose density Fraction 4 (Figure 4c-d, Supplementary Figure S7c-d) as did PiMDP2-mCitrine
446 and Pi04314-mCherry co-expressed in transgenic *P. infestans* (Figure 4e-f, Supplementary
447 Figure S7e-f). Moreover, a transgenic line co-expressing both MARVEL domain proteins

448 demonstrated that mCherry-PiMDP1 and PiMDP2-mCitrine both accumulated primarily in
449 Fraction 4 (Figure 4g-h, Supplementary Figure S7g-h). Fraction 4 correlates with the density
450 that EVs such as exosomes are expected to be buoyant (1.13-1.19 g/ml), according to the
451 literature (Colombo et al. 2014). Nanoparticle tracking analysis (NTA) of the sucrose fractions
452 indicated that the largest concentration of nanoparticles appeared in Fraction 4 with a main
453 peak sizes of approximately 80 nm diameter and a smaller peak of approximately 180 nm
454 (Figure 4i). Few nanoparticles were observed in Fractions 1 and 2; Fraction 3 had a small peak
455 around 140nm and there was a low level mixture of larger sized material in Fractions 5 and 6.
456 In agreement with this, TEM images showed no EVs in Fraction 1 (Figure 4j), as a control,
457 whereas many EV-like vesicle structures were observed in Fraction 4 samples (Figure 4k).

458 **3.4 MARVEL domain proteins co-localise frequently with RxLR Pi04314 at hyphal vesicles *in***
459 ***vitro***

460 After establishing that the MARVEL EV marker candidates co-accumulate with RxLR Pi04314
461 in Sucrose Fraction 4 that has been demonstrated to contain EV structures by NTA and TEM,
462 the localisation of these proteins inside *P. infestans* hyphae was examined to determine
463 whether they also co-associated with vesicles prior to secretion. Firstly, hyphae from a
464 transgenic line co-expressing Pi04314-mCherry and the apoplastic effector/CWDE PiPE1-
465 mCitrine (Wang et al 2018), which does not accumulate in the EV pellet (Figure 2g), were
466 studied by confocal microscopy. As expected for two secreted proteins, both localised to
467 vesicle-like structures inside the hyphae but fluorescence intensity plots drawn through the
468 vesicles showed little co-localisation of the two proteins (Figure 5a-b, Supplementary Figure
469 S8a, S9). A transgenic line co-expressing two independent RxLRs, Pi04314-mCherry and
470 Pi09216-mCitrine, was examined and both effectors strongly co-localised to the same vesicle-
471 like structures inside the hyphae, suggesting that they may follow the same secretory pathway
472 (Figure 5c, 5d, Supplementary Figure S8b, S9). EV marker candidates PiMDP1-mCitrine and
473 PiMDP2-mCitrine were both observed to localise to the plasma membrane (PM) as well as to
474 many vesicle-like structures inside the hyphae (Figure 5e, 5g & i, Supplementary Figure S8c-
475 e). Fluorescence intensity plots through the hyphae demonstrate PiMDP1-mCitrine and
476 Pi04314-mCherry showed the same strong levels of colocalisation to vesicles as the two RXLR
477 effectors (Figure 5e-f, Supplementary Figure S8c, S9). PiMDP2-mCitrine and Pi04314-mCherry
478 also co-localised to a subset of vesicles, albeit to lower levels than PiMDP1-mCitrine and

479 Pi04314-mCherry (Figure 5g-h, Supplementary Figure S8d, S9). In addition, when mCherry-
480 PiMDP1 and PiMDP2-mCitrine were co-expressed *in vitro* both localise to subsets of
481 overlapping and distinct vesicle-like structures in hyphae (Figure 5i-j, Supplementary Figure
482 S8e, S9). Together, this suggests that there is a mixed population of vesicles containing diverse
483 cargoes that may have different functions and distinctive transit routes. To further confirm the
484 identity of the vesicle-like structures observed in the hyphae endo-vesicles were isolated from
485 *in vitro* grown hyphae expressing mCherry-PiMDP1 and PiMDP2-mCitrine (Reynolds et al.
486 2014; Wang et al. 2023b). The resulting pelleted endo-vesicles were found to contain the
487 tagged proteins by immunoblotting (Supplementary Figure S10a-b) and were observed to be
488 sensitive to the detergent triton, suggesting that the PiMDP1 and PiMDP2 markers are indeed
489 incorporated in membranous vesicles within hyphae.

490 **3.5 MARVEL-domain and RxLR effector proteins co-localise frequently at vesicles during**
491 **early infection**

492 As both MARVEL domain EV marker candidates were found to partially co-localise with RxLR
493 effector Pi04314 in vesicles inside *in vitro* grown hyphae, we examined their localisation
494 during early plant infection. To investigate this, we imaged hyphae just behind the leading
495 edge of infection, where haustoria were just starting to form and are represented by small
496 protrusions on the hyphae where RxLRs accumulate. Haustoria are specialised infection
497 structures produced by the pathogen and are the sites in closest association with the host.
498 These structures act as major sites of secretion for both pathogen and host (Wang et al. 2017,
499 2018; Boevink et al. 2020; Bozkurt and Kamoun 2020). In all cases Pi04314-mCherry was
500 observed to accumulate around the base of developing haustoria (Figure 6a-b, Supplementary
501 Figure S11) as has been reported in previous publications (Wang et al. 2017, 2018). Both
502 PiMDP1-mCitrine and PiMDP2-mCitrine were localised at the PM, including in the developing
503 haustorial membrane (HM) (Figure 6a-b, Supplementary Figure S11). In addition, fluorescence
504 intensity plots through the hyphae show that PiMDP1-mCitrine and Pi04314-mCherry (Figure
505 6a, Supplementary Figure S11a) and PiMDP2-mCitrine and Pi04314-mCherry (Figure 6b,
506 Supplementary Figure S11b) were observed to colocalise to a subset of vesicle-like structures
507 inside the hyphae but not every vesicle was found to contain both proteins, as was shown for
508 *P. infestans* hyphae *in vitro*. This agrees with the observations within *in vitro* grown hyphae,

509 providing further evidence of both shared and distinct vesicle trafficking and potential
510 downstream functions.

511 **3.6 PiMDP2 is enriched in the mature haustorial membrane during infection**

512 Later stages of infection, where the haustoria on *P. infestans* hyphae were mature and formed
513 elongated hook-like projections, were then examine by confocal microscopy. Here a striking
514 difference in the MARVEL-domain candidate EV marker localisation was observed. PiMDP1-
515 mCitrine was localised as before to the PM, HM and vesicles inside the hyphae (Figure 7a,
516 Supplementary Figure S12a). However, PiMDP2-mCitrine was found to accumulate strongly at
517 the HM (Figure 7b, Supplementary Figure S12b), although it was still observed weakly in the
518 PM and in vesicles. In both cases the co-expressed Pi04314-mCherry was found to be localised
519 around the base of the haustoria as expected. The difference in PiMDP2 localisation was
520 quantified by measuring the fluorescence intensity ratio of both PiMDP1-mCitrine and
521 PiMDP2-mCitrine in the HM relative to the PM in multiple images. While PiMDP1-mCitrine
522 found equally present in both membranes with a ratio of approximately 1, the fluorescence
523 of PiMDP2-mCitrine was significantly stronger in the HM with a higher mean ratio (Figure 7c).
524 This points to some possible differences in function between our EV candidate markers.

525

526 **4.0 DISCUSSION**

527 Differential ultracentrifugation is a common technique used to isolate EVs from different
528 organisms and tissues. Here, the pellet from ultracentrifugation (UC) of the culture media
529 used to grow *P. infestans* mycelia *in vitro* was demonstrated to contain EVs by both NTA and
530 TEM analyses (Figure 1). Proteomic analysis of the pelleted (EV-associated) material following
531 UC showed that it is enriched for both vesicle-associated and transmembrane proteins
532 compared to the supernatant (EV-independent) samples (Table 1), which is consistent with
533 the pellet containing EVs. Moreover, the pellets also contain proteins from filamentous plant
534 pathogens, such as coronin, which acts to regulate actin organisation and vesicle trafficking
535 during infection (Dulal et al. 2021; Li et al. 2019), as well as Rab7, a GTPase which regulates
536 effector secretion and membrane trafficking (Chen et al. 2023). Proteins which are notable in
537 their absence in the *P. infestans* EV-associated proteome are tetraspanins, which are typically
538 enriched in EVs in mammalian and plant systems (Cai et al. 2021; Van Niel et al. 2018).

539 Tetraspanins contain four TM helices and are used as molecular markers of EVs. They are
540 abundant, present in many different cell types and form stable tetraspanin-associated
541 microdomains. The availability of many monoclonal tetraspanin antibodies allows their
542 purification by immunoprecipitation thus facilitating studies of EV biogenesis, trafficking and
543 analysis of EV cargoes (Wang et al. 2024). The presence of EV markers is crucial to bring EV
544 research in oomycetes to the cutting edge.

545 Interestingly, tetraspanin homologues were also not identified in proteomic studies of EVs in
546 some fungi, so other molecular markers have been proposed. One such marker is SUR7 which
547 was found to be enriched in EVs from *Candida albicans* and *Zymoseptoria tritici* (Dawson et
548 al. 2020; Hill and Solomon 2020). SUR7 is a TM protein containing four TM helices and is a
549 component of the Membrane Compartment of Can1 (MCC)/eisosome, a specialised
550 microdomain at the fungal PM which forms stable membrane furrows (Lanze et al. 2020).
551 *SUR7* knockouts in *C. albicans* were shown to form smaller EVs with altered cargoes containing
552 less fungal virulence proteins (McKenna et al. 2023). The MCC/eisosome is involved in many
553 different membrane processes, including membrane integrity, lipid regulation, maintaining
554 nutrient transporters at the PM, and responses to stress, as well as impacting fungal virulence
555 (Lanze et al. 2020). Another component of the MCC/eisosome is Non Classical Export
556 (NCE)102 which was also found to be enriched in fungal EVs (Dawson et al. 2020). In addition
557 to being part of the MCC/eisosome, NCE102 is reportedly involved in unconventional protein
558 secretion in yeast (Cleves et al. 1996). NCE102 is a MAL And Related proteins for VEsicle
559 formation and membrane Link (MARVEL) domain-containing protein. A MARVEL domain
560 consists of four TM helices and the best characterised mammalian family members are
561 involved in membrane trafficking, transcytosis and cell signalling (Sánchez-Pulido et al. 2002;
562 Li et al. 2024). Plant pathogenic fungus *Alternaria brassicicola* in which AbNCE102 was
563 mutated had a reduced ability to colonise its host *B. oleracea,* possibly due to the significant
564 reduction in the formation of appressoria-like structures required for invasion (Colou et al.
565 2019). Like NCE102, PiMDP1 and PiMDP2 are PM-localised and are enriched in EVs. However,
566 they possess two MARVEL domains and so contain eight TM helices. Human MARVEL protein
567 MYADM also contains two MARVEL domains, is PM localised alongside the Rho GTPase Rac
568 and is involved in membrane organisation, cell spreading and migration (Aranda et al. 2011;
569 Labat-de-Hoz et al. 2023). Moreover, MYADM acts as a receptor required for entry of human

570 parechovirus PeV-A (Qiao et al. 2024) and has been proposed as a molecular marker of EVs
571 from plasma (Hu et al. 2024).

572 Although tetraspanins were not observed in our EV proteome, they were observed in a
573 reported EV proteome for *Phytophthora sojae* (Zhu et al 2023). It is not clear why tetraspanins
574 were absent in our EV dataset, although growth conditions were different. However, of the 50
575 most abundant non-ribosomal proteins in our EV proteome (Supplementary Table S2),
576 candidate orthologues of 19 (38%) were represented in the *P. sojae* EV proteome
577 (Supplementary Table S4). Importantly, the *P. sojae* orthologue of PiMDP1 (Ps_341763) was
578 represented in the *P. sojae* EV proteome (Zhu et al 2023), indicating that it is a potential EV
579 marker also for that pathogen.

580 **The Role of Unconventional Protein Secretion (UPS) in Filamentous Plant Pathogens**

581 The secretion of EVs is known to be one form of UPS which normally occurs for proteins which
582 do not contain a signal peptide (SP). This study used proteomic analysis to identify proteins
583 secreted into the culture media used to grow *P. infestans*. Of the proteins identified as
584 enriched in the supernatant 35% were predicted to contain an SP which included many
585 apoplastic effectors and CWDE known to be conventionally secreted. Only 8% of proteins
586 found to be enriched in the pellet contained an SP, many of which included RxLR effectors
587 which have been reported to be unconventionally secreted (Wang et al. 2018, 2017; Xu 2023).
588 This suggests that UPS contributes significantly to the *P. infestans* secretome. Indeed the EV
589 pellet proteome exhibits some of the hallmarks of UPS and includes proteins such as ATG9
590 which is associated with autophagosomes but also with Compartments for UPS (CUPS) (Bruns
591 et al. 2011; New and Thomas 2019). The pellet also contains the vacuolar sorting receptor BP-
592 80, which is associated with multivesicular bodies (MVBs) that have been implicated in the
593 biogenesis of EVs which play a role in plant pathogen interactions (Zhuang et al. 2024; Cai et
594 al. 2021). UPS has been suggested to play an important role in filamentous plant pathogens
595 with a large proportion of secreted proteins found to lack an SP in *Magnaporthe*, *Fusarium*,
596 *Trichoderma* and *Phytophthora*. Moreover, increases of UPS in these pathogens have been
597 reported during abiotic stress and notably during infection (Stuer et al. 2023).

598 **Multiple Secretory Pathways**

599 RxLR Pi04314 and apoplastic effector/CWDE pectinesterase 1 (PiPE1) were observed to
600 localise to distinct vesicles inside plant hyphae suggesting that they are exported by different
601 secretion pathways, in line with previous observations (Wang et al. 2018). However, co-
602 expression of the RxLR effectors Pi04314 and Pi09216 revealed them to display predominant
603 co-localisation to the same vesicles suggesting a common secretory pathway (Figure 5,
604 Supplementary Figure S8a-b, S9). In the case of candidate EV markers PiMDP1 and PiMDP2
605 there is frequent but not complete co-localisation at vesicles in hyphae *in vitro* and *in planta*
606 with the RXLR Pi04314 and, indeed, with each other (Figures 5-6, Supplementary Figures S8
607 & S9, S11). This makes a case for the existence of both distinct and overlapping pathways for
608 vesicle export. It is also possible that Pi04314 is associated with different vesicles prior to its
609 association with PiMDP-marked vesicles. The fact that both PiMDP1 and PiMDP2 are
610 predominantly found, alongside Pi04314, in sucrose density fractions indicative of EV
611 accumulation (1.13-1.19 g/ml; Colombo et al 2014), where we observe many vesicular
612 structures by TEM and NTA, plus both markers are vulnerable to treatment with detergent
613 (Figures 3, 4, Supplementary Figure S10), suggests that they are indeed associated with
614 membranous structures such as EVs. Interestingly during *in planta* colonisation there are signs
615 of diverging functional roles for PiMDP1 and PiMDP2, as the latter shares a gene expression
616 pattern with virulence factors such as Pi04314 (Figure 3c; Supplementary Figure S5) and is
617 thus associated with the biotrophic phase of *P. infestans* infection, when both pathogen and
618 host are interacting closely via the haustorial interface. By contrast, *PiMDP1* gene expression
619 steadily increases throughout infection from biotrophy into necrotrophy. Moreover, PiMDP2
620 but not PiMDP1 accumulates strongly in the mature haustorial membrane (HM) (Figure 7,
621 Supplementary Figure S12). Such enrichment of PiMDP2 at the HM could be consistent with
622 its accumulation as a result of vesicle fusion during secretion.

623 A previous study has shown that RxLRs can be taken up by plants via clathrin-mediated
624 endocytosis (CME) (Wang et al. 2023b, 2023a). Indeed, there is some overlap (34%) in the
625 RxLRs identified in the proteomics of immune-purified endosomes and those identified in this
626 study in the EV pellet proteome (Supplementary Table S5). One question is how is such
627 endocytosis triggered? The recognition and binding of PAMPs by their cognate receptors, such
628 as the binding of flg22 by FLS2, is known to induce CME of the receptor (Mbengue et al. 2016).
629 The majority of PAMPs identified in this study were abundantly represented in the

630 supernatant. However, some were enriched in the EV pellet. Further work is needed to
631 determine whether such PAMPs are exposed on the surface of EVs and so trigger uptake
632 through binding to pattern recognition receptors on the host PM. Interestingly, although our
633 study did not reveal tetraspanins (TETs), TETs associated with *P. sojae* EVs were found to be
634 recognised as PAMPs by host and nonhost plants (Zhu et al. 2023).

635 **EVs Associated with Virulence Factors**

636 It is attractive to hypothesise that secretion of proteins such as virulence factors may be best
637 achieved by coordinating their delivery to precise locations through their packaging into EVs.
638 42 RXLR effector proteins were detected in our *in vitro* study of the EV proteome. This is
639 remarkable, given that the genes encoding these virulence proteins are transcriptionally up-
640 regulated during infection (e.g. Whisson et al 2007). However, one explanation for their
641 detection is that, despite the likely low basal expression level of many of these RXLR effectors,
642 enriching for an EV pellet co-enriched 33 RXLRs to detectable levels. Future work will hopefully
643 enable pathogen EVs to be immuno-isolated from infection, using tagged marker proteins
644 such as PiMDPs revealed in this study. This will allow us to better determine the protein
645 cargoes and composition of EVs during infection.

646 Consistent with our study of *in vitro* EVs from *P. infestans*, proteomic analysis of EVs from the
647 plant pathogen *Fusarium graminearum* identified a collection of both existing and novel
648 candidate effector proteins and virulence factors associated with EVs (Garcia-Ceron et al.
649 2021). Infiltration of plants with EVs from *F. oxysporum* f. sp. *vasinfectum* led to host cell death
650 (Bleackley et al. 2020). Also in oomycete research, *P. capsici* EVs enhanced virulence when
651 applied to leaves (Fang et al. 2021). Identifying molecular markers associated with EVs, such
652 as PiMDP1 and PiMDP2, especially those EVs also associated with virulence factors, will be
653 important to dissect secretion pathways required for infection. Such markers also provide
654 novel agrochemical control targets. This study provides a large dataset of EV pellet-associated
655 proteins which can be dissected by the community to determine if useful markers for EV
656 biogenesis, distinct secretion pathways, and thus targets for disease control, can be identified.

657 **Acknowledgements**

658 We thank Prof Simon Powis from the University of St Andrews for his expertise and use of
659 Nanoparticle tracking equipment. We thank also Prof Alex Jones, Warwick University, for
660 helpful guidance in analysing proteomic data.

661 **Funding**

662 This research was supported by Biotechnology and Biological Sciences Research Council grant
663 BB/S003096/1; European Research Council (ERC)-Advanced grant PathEVome (787764); and
664 Scottish Government Rural and Environment Science and Analytical Services Division (RESAS)
665 JHI B1-1. WW was supported by the China Scholarship Council (CSC).

666 **Author contributions**

667 S.B., H.M., W.W., S.C.W., P.C.B., and P.R.J.B. conceived of and designed the research; H.M., S.B.,
668 W.W., P.C.B., L.W., J.P., SW., and S.C.W performed the research; S.B., H.M., W.W., J.P., S.W., and
669 S.C.W. contributed new reagents/analytic tools; S.B., H.M., P.C.B., S.C.W., W.W., and P.R.J.B.
670 analysed data; P.R.J.B., S.C.W. and P.C.B. won funding for the research; and H.M., S.B, P.C.B and
671 P.R.J.B. wrote the paper with input from all co-authors.

672 The authors declare no competing interest.

673

674 **References**

675 Ah-Fong, A. M. V., and Judelson, H. S. 2011. Vectors for fluorescent protein tagging in
676 Phytophthora: Tools for functional genomics and cell biology. Fungal Biol. 115:882–890

677 Aranda, J. F., Reglero-Real, N., Kremer, L., Marcos-Ramiro, B., Ruiz-Sáenz, A., Calvo, M.,
678 Enrich, C., Correas, I., Millán, J., and Alonso, M. A. 2011. MYADM regulates Rac1
679 targeting to ordered membranes required for cell spreading and migration. Mol. Biol.
680 Cell. 22:1252–1262

681 Bleackley, M. R., Samuel, M., Garcia-Ceron, D., McKenna, J. A., Lowe, R. G. T., Pathan, M.,
682 Zhao, K., Ang, C. S., Mathivanan, S., and Anderson, M. A. 2020. Extracellular Vesicles
683 From the Cotton Pathogen Fusarium oxysporum f. sp. vasinfectum Induce a Phytotoxic
684 Response in Plants. Front. Plant Sci. 10

685 Boevink, P. C., Birch, P. R. J., Turnbull, D., and Whisson, S. C. 2020. Devastating intimacy: the

686 cell biology of plant–Phytophthora interactions. New Phytol. 228:445–458

687 Bozkurt, T. O., and Kamoun, S. 2020. The plant–pathogen haustorial interface at a glance. J.
688 Cell Sci. 133

689 Bruns, C., Mccaffery, J. M., Curwin, A. J., Duran, J. M., and Malhotra, V. 2011. Biogenesis of a
690 novel compartment for autophagosome-mediated unconventional protein secretion. J.
691 Cell Biol. 195:979–992

692 Cai, Q., He, B., Wang, S., Fletcher, S., Niu, D., Mitter, N., Birch, P. R. J., and Jin, H. 2021.
693 Message in a Bubble: Shuttling Small RNAs and Proteins between Cells and Interacting
694 Organisms Using Extracellular Vesicles. Annu. Rev. Plant Biol. 72:497–524

695 Cai, Q., Qiao, L., Wang, M., He, B., Lin, F. M., Palmquist, J., Huang, S. Da, and Jin, H. 2018.
696 Plants send small RNAs in extracellular vesicles to fungal pathogen to silence virulence
697 genes. Science (80-.). 360:1126–1129

698 Chen, X., Selvaraj, P., Lin, L., Fang, W., Wu, C., Yang, P., Zhang, J., Abubakar, Y. S., Yang, F.,
699 Lu, G., Liu, W., Wang, Z., Naqvi, N. I., and Zheng, W. 2023. Rab7/Retromer-based
700 endolysosomal trafficking is essential for proper host invasion in rice blast. New Phytol.
701 239:1384–1403

702 Cleves, A. E., Cooper, D. N. W., Barondes, S. H., and Kelly, R. B. 1996. A new pathway for
703 protein export in Saccharomyces cerevisiae. J. Cell Biol. 133:1017–1026

704 Colombo, M., Raposo, G., and Théry, C. 2014. Biogenesis, secretion, and intercellular
705 interactions of exosomes and other extracellular vesicles. Annu. Rev. Cell Dev. Biol.
706 30:255–289

707 Colou, J., N'Guyen, G. Q., Dubreu, O., Fontaine, K., Kwasiborski, A., Bastide, F., Manero, F.,
708 Hamon, B., Aligon, S., Simoneau, P., and Guillemette, T. 2019. Role of membrane
709 compartment occupied by Can1 (MCC) and eisosome subdomains in plant
710 pathogenicity of the necrotrophic fungus Alternaria brassicicola. BMC Microbiol. 19:1–
711 14

712 Dawson, C. S., Garcia-Ceron, D., Rajapaksha, H., Faou, P., Bleackley, M. R., and Anderson, M.
713 A. 2020. Protein markers for Candida albicans EVs include claudin-like Sur7 family

714 proteins. J. Extracell. Vesicles. 9:1750810

715 Dereeper, A., Guignon, V., Blanc, G., Audic, S., Buffet, S., Chevenet, F., Dufayard, J. F.,
716 Guindon, S., Lefort, V., Lescot, M., Claverie, J. M., and Gascuel, O. 2008. Phylogeny.fr:
717 robust phylogenetic analysis for the non-specialist. Nucleic Acids Res. 36:W465–W469

718 Doellinger, J., Blumenscheit, C., Schneider, A., and Lasch, P. 2020. Isolation Window
719 Optimization of Data-Independent Acquisition Using Predicted Libraries for Deep and
720 Accurate Proteome Profiling. Anal. Chem. 92:12185–12192

721 Dulal, N., Rogers, A. M., Proko, R., Bieger, B. D., Liyanage, R., Krishnamurthi, V. R., Wang, Y.,
722 and Egan, M. J. 2021. Turgor-dependent and coronin-mediated F-actin dynamics drive
723 septin disc-to-ring remodeling in the blast fungus Magnaporthe oryzae. J. Cell Sci.
724 134:jcs251298

725 Fang, Y., Wang, Z., Zhang, S., Peng, Q., and Liu, X. 2021. Characterization and proteome
726 analysis of the extracellular vesicles of Phytophthora capsici. J. Proteomics. 238:104137

727 Garcia-Ceron, D., Lowe, R. G. T., McKenna, J. A., Brain, L. M., Dawson, C. S., Clark, B.,
728 Berkowitz, O., Faou, P., Whelan, J., Bleackley, M. R., and Anderson, M. A. 2021.
729 Extracellular Vesicles from Fusarium graminearum Contain Protein Effectors Expressed
730 during Infection of Corn. J. Fungi. 7:977

731 Giraldo, M. C., and Valent, B. 2013. Filamentous plant pathogen effectors in action. Nat. Rev.
732 Microbiol. 2013 1111. 11:800–814

733 Haas, B. J., Kamoun, S., Zody, M. C., Jiang, R. H. Y., Handsaker, R. E., Cano, L. M., Grabherr,
734 M., Kodira, C. D., Raffaele, S., Torto-Alalibo, T., Bozkurt, T. O., Ah-Fong, A. M. V.,
735 Alvarado, L., Anderson, V. L., Armstrong, M. R., Avrova, A., Baxter, L., Beynon, J.,
736 Boevink, P. C., Bollmann, S. R., Bos, J. I. B., Bulone, V., Cai, G., Cakir, C., Carrington, J. C.,
737 Chawner, M., Conti, L., Costanzo, S., Ewan, R., Fahlgren, N., Fischbach, M. A., Fugelstad,
738 J., Gilroy, E. M., Gnerre, S., Green, P. J., Grenville-Briggs, L. J., Griffith, J., Grünwald, N.
739 J., Horn, K., Horner, N. R., Hu, C. H., Huitema, E., Jeong, D. H., Jones, A. M. E., Jones, J.
740 D. G., Jones, R. W., Karlsson, E. K., Kunjeti, S. G., Lamour, K., Liu, Z., Ma, L., MacLean, D.,
741 Chibucos, M. C., McDonald, H., McWalters, J., Meijer, H. J. G., Morgan, W., Morris, P. F.,
742 Munro, C. A., O'Neill, K., Ospina-Giraldo, M., Pinzón, A., Pritchard, L., Ramsahoye, B.,

743 Ren, Q., Restrepo, S., Roy, S., Sadanandom, A., Savidor, A., Schornack, S., Schwartz, D.
744 C., Schumann, U. D., Schwessinger, B., Seyer, L., Sharpe, T., Silvar, C., Song, J.,
745 Studholme, D. J., Sykes, S., Thines, M., Van De Vondervoort, P. J. I., Phuntumart, V.,
746 Wawra, S., Weide, R., Win, J., Young, C., Zhou, S., Fry, W., Meyers, B. C., Van West, P.,
747 Ristaino, J., Govers, F., Birch, P. R. J., Whisson, S. C., Judelson, H. S., and Nusbaum, C.
748 2009. Genome sequence and analysis of the Irish potato famine pathogen
749 Phytophthora infestans. Nat. 2009 4617262. 461:393–398

750 He, B., Wang, H., Liu, G., Chen, A., Calvo, A., Cai, Q., and Jin, H. 2023. Fungal small RNAs ride
751 in extracellular vesicles to enter plant cells through clathrin-mediated endocytosis. Nat.
752 Commun. 14:4383

753 Hill, E. H., and Solomon, P. S. 2020. Extracellular vesicles from the apoplastic fungal wheat
754 pathogen Zymoseptoria tritici. Fungal Biol. Biotechnol. 7:13

755 Hu, L., Zheng, X., Zhou, M., Wang, J., Tong, L., Dong, M., Xu, T., and Li, Z. 2024. Optimized
756 AF4 combined with density cushion ultracentrifugation enables profiling of high-purity
757 human blood extracellular vesicles. J. Extracell. Vesicles. 13:e12470

758 Judelson, H. S., Tyler, B. M., and Michelmore, R. W. 1991. Transformation of the oomycete
759 pathogen, Phytophthora infestans. Mol. Plant. Microbe. Interact. 4:602–607

760 Kamoun, S., Furzer, O., Jones, J. D. G., Judelson, H. S., Ali, G. S., Dalio, R. J. D., Roy, S. G.,
761 Schena, L., Zambounis, A., Panabières, F., Cahill, D., Ruocco, M., Figueiredo, A., Chen, X.
762 R., Hulvey, J., Stam, R., Lamour, K., Gijzen, M., Tyler, B. M., Grünwald, N. J., Mukhtar,
763 M. S., Tomé, D. F. A., Tör, M., Van Den Ackerveken, G., Mcdowell, J., Daayf, F., Fry, W.
764 E., Lindqvist-Kreuze, H., Meijer, H. J. G., Petre, B., Ristaino, J., Yoshida, K., Birch, P. R. J.,
765 and Govers, F. 2015. The Top 10 oomycete pathogens in molecular plant pathology.
766 Mol. Plant Pathol. 16:413–434

767 Labat-de-Hoz, L., Rubio-Ramos, A., Correas, I., and Alonso, M. A. 2023. The MAL Family of
768 Proteins: Normal Function, Expression in Cancer, and Potential Use as Cancer
769 Biomarkers. Cancers (Basel). 15:2801

770 Lacomme, C., Hrubikova, K., Journal, I. H.-T. P., and 2003, undefined. 2003. Enhancement of
771 virus-induced gene silencing through viral-based production of inverted-repeats. Wiley

772 Online Libr. Lacomme, K Hrubikova, I HeinThe Plant Journal, 2003•Wiley Online Libr.
773 34:543–553

774 Lanze, C. E., Gandra, R. M., Foderaro, J. E., Swenson, K. A., Douglas, L. M., and Konopka, J. B.
775 2020. Plasma Membrane MCC/Eisosome Domains Promote Stress Resistance in Fungi.
776 Microbiol. Mol. Biol. Rev. 84:e00063-19

777 Li, M., Du, Y., Zhang, X., and Zhou, W. 2024. Research advances of MAL family members in
778 tumorigenesis and tumor progression (Review). Mol. Med. Rep. 29:57

779 Li, X., Zhong, K., Yin, Z., Hu, J., Wang, W., Li, L., Zhang, H., Zheng, X., Wang, P., and Zhang, Z.
780 2019. The seven transmembrane domain protein MoRgs7 functions in surface
781 perception and undergoes coronin MoCrn1-dependent endocytosis in complex with Gα
782 subunit MoMagA to promote cAMP signaling and appressorium formation in
783 Magnaporthe oryzae. PLOS Pathog. 15:e1007382

784 Lin, X., Wang, S., de Rond, L., Bertolin, N., Wouters, R. H. M., Wouters, D., Domazakis, E.,
785 Bitew, M. K., Win, J., Dong, S., Visser, R. G. F., Birch, P., Kamoun, S., and Vleeshouwers,
786 V. G. A. A. 2020. Divergent evolution of pcf/scr74 effectors in oomycetes is associated
787 with distinct recognition patterns in solanaceous plants. MBio. 11:1–12

788 Mbengue, M., Bourdais, G., Gervasi, F., Beck, M., Zhou, J., Spallek, T., Bartels, S., Boller, T.,
789 Ueda, T., Kuhn, H., and Robatzek, S. 2016. Clathrin-dependent endocytosis is required
790 for immunity mediated by pattern recognition receptor kinases. Proc. Natl. Acad. Sci. U.
791 S. A. 113:11034–11039

792 McKenna, J. A., Garcia-Ceron, D., Bleackley, M. R., Yu, L., Bulone, V., and Anderson, M. A.
793 2023. SUR7 deletion in Candida albican s impacts extracellular vesicle features and
794 delivery of virulence factors. J. Extracell. Biol. 2:e82

795 New, J., and Thomas, S. M. 2019. Autophagy-dependent secretion: mechanism, factors
796 secreted, and disease implications. Autophagy. 15:1682–1693

797 Van Niel, G., D'Angelo, G., and Raposo, G. 2018. Shedding light on the cell biology of
798 extracellular vesicles. Nat. Rev. Mol. Cell Biol. 19:213–228

799 Oliveira-Garcia, E., Tamang, T. M., Park, J., Dalby, M., Martin-Urdiroz, M., Herrero, C. R., Vu,

800 A. H., Park, S., Talbot, N. J., and Valent, B. 2023. Clathrin-mediated endocytosis
801 facilitates the internalization of Magnaporthe oryzae effectors into rice cells. Plant Cell.
802 35:2527–2551

803 Qiao, W., Richards, C. M., Kim, Y., Zengel, J. R., Ding, S., Greenberg, H. B., and Carette, J. E.
804 2024. MYADM binds human parechovirus 1 and is essential for viral entry. Nat.
805 Commun. 15:3469

806 Reynolds, G. D., August, B., and Bednarek, S. Y. 2014. Preparation of enriched plant clathrin-
807 coated vesicles by differential and density gradient centrifugation. Methods Mol. Biol.
808 1209:163–177

809 Rutter, B. D., and Innes, R. W. 2017. Extracellular vesicles isolated from the leaf apoplast
810 carry stress-response proteins. Plant Physiol. 173:728–741

811 Sabbadin, F., Urresti, S., Henrissat, B., Avrova, A. O., Welsh, L. R. J., Lindley, P. J., Csukai, M.,
812 Squires, J. N., Walton, P. H., Davies, G. J., Bruce, N. C., Whisson, S. C., and McQueen-
813 Mason, S. J. 2021. Secreted pectin monooxygenases drive plant infection by pathogenic
814 oomycetes. Science (80-.). 373:774–779

815 Sánchez-Pulido, L., Martín-Belmonte, F., Valencia, A., and Alonso, M. A. 2002. MARVEL: a
816 conserved domain involved in membrane apposition events. Trends Biochem. Sci.
817 27:599–601

818 Stuer, N., Van Damme, P., Goormachtig, S., and Van Dingenen, J. 2023. Seeking the
819 interspecies crosswalk for filamentous microbe effectors. Trends Plant Sci. 28:1045–
820 1059

821 Tiwari, I., Shah, K. K., Tripathi, S., Modi, B., Subedi, S., and Shrestha, J. 2021. Late blight of
822 potato and its management through the application of different fungicides and organic
823 amendments: a review. J. Agric. Nat. Resour. 4:301–320

824 Wang, H., Oliveira-Garcia, E., Boevink, P. C., Talbot, N. J., Birch, P. R. J., and Valent, B. 2023a.
825 Filamentous pathogen effectors enter plant cells via endocytosis. Trends Plant Sci.
826 28:1214–1217

827 Wang, H., Wang, S., Wang, W., Xu, L., Welsh, L. R. J., Gierlinski, M., Whisson, S. C., Hemsley,

828 P. A., Boevink, P. C., and Birch, P. R. J. 2023b. Uptake of oomycete RXLR effectors into
829 host cells by clathrin-mediated endocytosis. Plant Cell. 35:2504–2526

830 Wang, S., Boevink, P. C., Welsh, L., Zhang, R., Whisson, S. C., and Birch, P. R. J. 2017. Delivery
831 of cytoplasmic and apoplastic effectors from phytophthora infestans haustoria by
832 distinct secretion pathways. New Phytol. 216:205–215

833 Wang, S., He, B., Wu, H., Cai, Q., Ramírez-Sánchez, O., Abreu-Goodger, C., Birch, P. R. J., and
834 Jin, H. 2024. Plant mRNAs move into a fungal pathogen via extracellular vesicles to
835 reduce infection. Cell Host Microbe. 32:93-105.e6

836 Wang, S., McLellan, H., Boevink, P. C., and Birch, P. R. J. 2023c. RxLR Effectors: Master
837 Modulators, Modifiers and Manipulators. Mol. Plant-Microbe Interact. 36:754–763

838 Wang, S., Welsh, L., Thorpe, P., Whisson, S. C., Boevink, P. C., and Birch, P. R. J. 2018. The
839 Phytophthora infestans haustorium is a site for secretion of diverse classes of infection-
840 associated proteins. MBio. 9:e01216-18.

841 Welsh LRJ, Whisson SC. 2025;2892:35-47. Methods Mol Biol. doi: 10.1007/978-1-0716-4330-
842 3_3.

843 Whisson, S. C., Boevink, P. C., Moleleki, L., Avrova, A. O., Morales, J. G., Gilroy, E. M.,
844 Armstrong, M. R., Grouffaud, S., Van West, P., Chapman, S., Hein, I., Toth, I. K.,
845 Pritchard, L., and Birch, P. R. J. 2007. A translocation signal for delivery of oomycete
846 effector proteins into host plant cells. Nature. 450:115–118

847 Xu, L. 2023. Exploring the role of the RXLR-EER motifs in the secretion and translocation
848 processes of Phytophthora infestans cytoplasmic effectors. PhD Thesis, University of
849 Dundee.

850 Zheng, J.F., Ge, Q.W., Yan, Y.C., Zhang, X.P., Huang, L., Yin, Y.B. 2023. dbCAN3: automated
851 carbohydrate-active enzyme and substrate annotation. Nucleic Acids Res. 51: W115–
852 W121

853 Zhu, J., Qiao, Q., Sun, Y., Xu, Y., Shu, H., Zhang, Z., Liu, F., Wang, H., Ye, W., Dong, S., Wang,
854 Y., Ma, Z., and Wang, Y. 2023. Divergent sequences of tetraspanins enable plants to
855 specifically recognize microbe-derived extracellular vesicles. Nat. Commun. 14:4877

Zhuang, X., Li, R., and Jiang, L. 2024. A century journey of organelles research in the plant endomembrane system. Plant Cell. 36:1312–1333

Table 1: Enrichment of proteins of interest in the pellet vs the supernatant

Type of Protein	Non Significant	Pellet Enriched	Supt Enriched	Total
All proteins	62	1009	255	1326
RxLRs	3	33	6	42
Apoplastic	0	1	7	8
Vesicle-associated	1	38	2	41
CWDE	1	11	34	46
TM	2	71	8	81
PAMPS	1	4	8	13
Signal Peptide	11	63	81	155
SP +TM	0	22	6	28

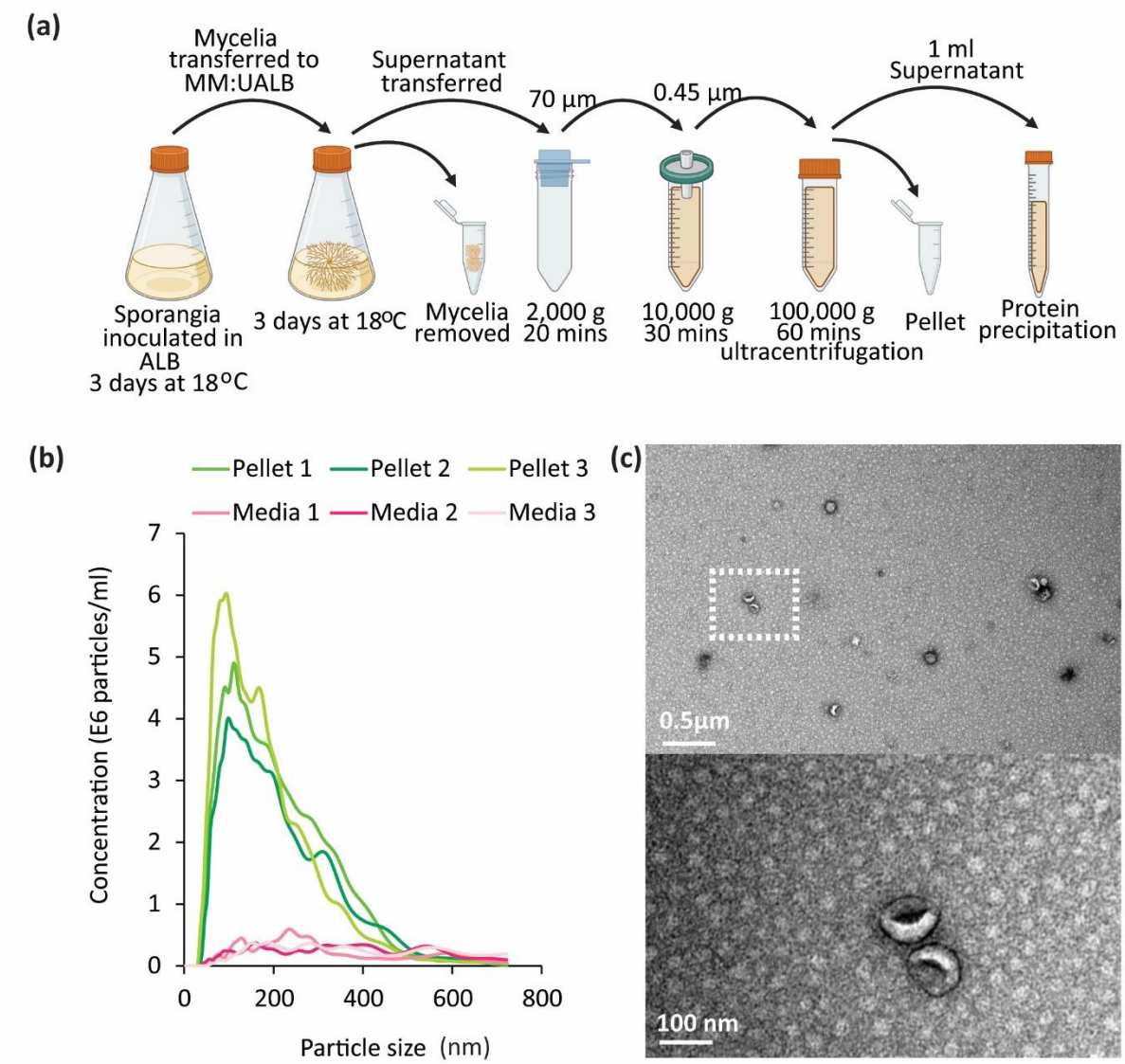

Figure 1: *Phytophthora infestans* secretes extracellular vesicle like particles into growth media. (a) Schematic representation of the ultracentrifugation protocol used for nanoparticle isolation to generate the crude pellet from *P. infestans* inoculated media. Schematic made in BioRender. (b) Nanoparticle tracking (NTA) data showing the size distribution of particles in the crude nanoparticle pellet from *P. infestans*-inoculated media and the pellet from uninoculated control media. Results from three independent replicates of each inoculated and uninoculated control are shown in the line graph. (c) Transmission electron microscopy negative stain images showing vesicles present within the nanoparticle crude pellet isolated from *P. infestans* inoculated media. Top image scale bar represents 0.5 µm. Dashed box represents the location of the higher magnification image below where the scale bar represents 100 nm.

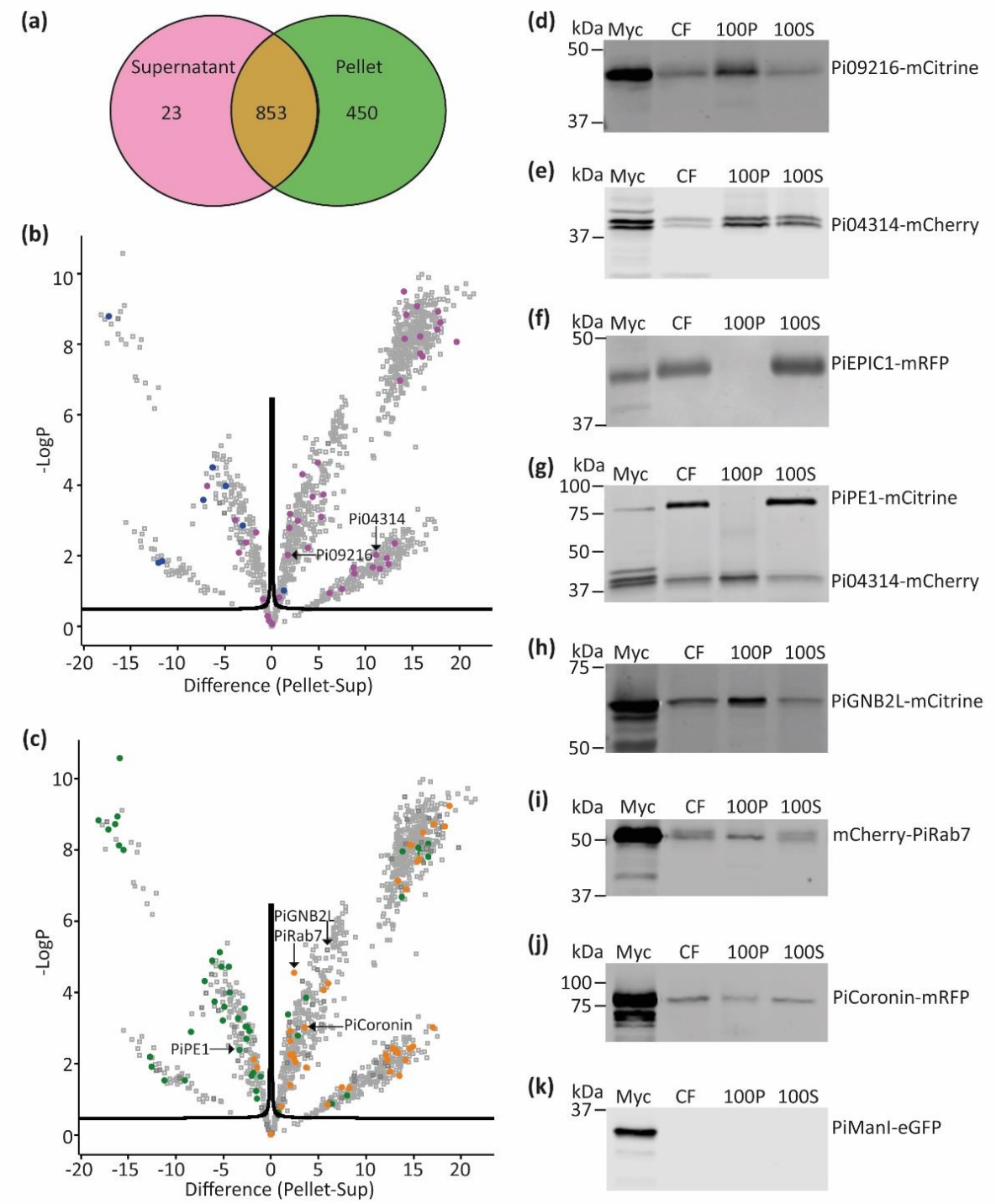

Figure 2: Overview of the *P. infestans* crude vesicle pellet proteome. (a) Venn diagram showing the distribution of proteins between the supernatant and pellet samples after crude extracellular vesicle pellet isolation and LC-MS/MS analysis from *P. infestans*-inoculated media. (b) Volcano plot showing the statistical distribution of proteins within the pellet vs supernatant samples. Pink spots indicate RxLR motif-containing effector proteins, blue spots represent apoplastic effector proteins. Black arrows highlight RxLR proteins of interest. (c) The same volcano plot with green spots indicating cell wall degrading enzymes (CWDE), orange spots indicating vesicle-associated proteins. Black arrows highlight CWDE and vesicle-associated proteins of interest. CWDE were identified using dbCAN3 (https://bcb.unl.edu/dbCAN2/). (d-k) Immunoblots of crude vesicle pellet and supernatant isolation from multiple transgenic *P. infestans* lines expressing mRFP, mCherry or mCitrine tagged proteins of

888 interest. The membranes were probed with αRFP for mRFP or mCherry fusions, or αGFP for mCitrine
889 fusions. These western blots show mycelia (Myc) and culture filtrate (CF) samples prior to any
890 centrifugation, 100,000 x*g* pellet (100P) and supernatant samples after 100,000 x*g* spin (100S). These
891 western blots confirm the distribution of the proteins based on the observations from the volcano
892 plots (b-c). The proteins of interest expressed in the P. infestans isolates are (d) RxLR effector Pi09216-
893 mCitrine. (e) RxLR effector Pi04314-mCherry. (f) apoplastic effector PiEPIC1-mRFP. (g) CWDE
894 Pectinesterase 1 (PiPE1-mCitrine) and RxLR effector Pi04314-mCherry. (h) vesicle associated protein
895 Guanine nucleotide-binding protein subunit β-2-like (PiGNB2L)-mCitrine. (i) vesicle associated protein
896 PiRab7-mCherry. (j) vesicle associated protein PiCoronin-mRFP. (k) the control Golgi marker protein
897 PiManI-eGFP (Ah-Fong and Judelson, 2011).

898

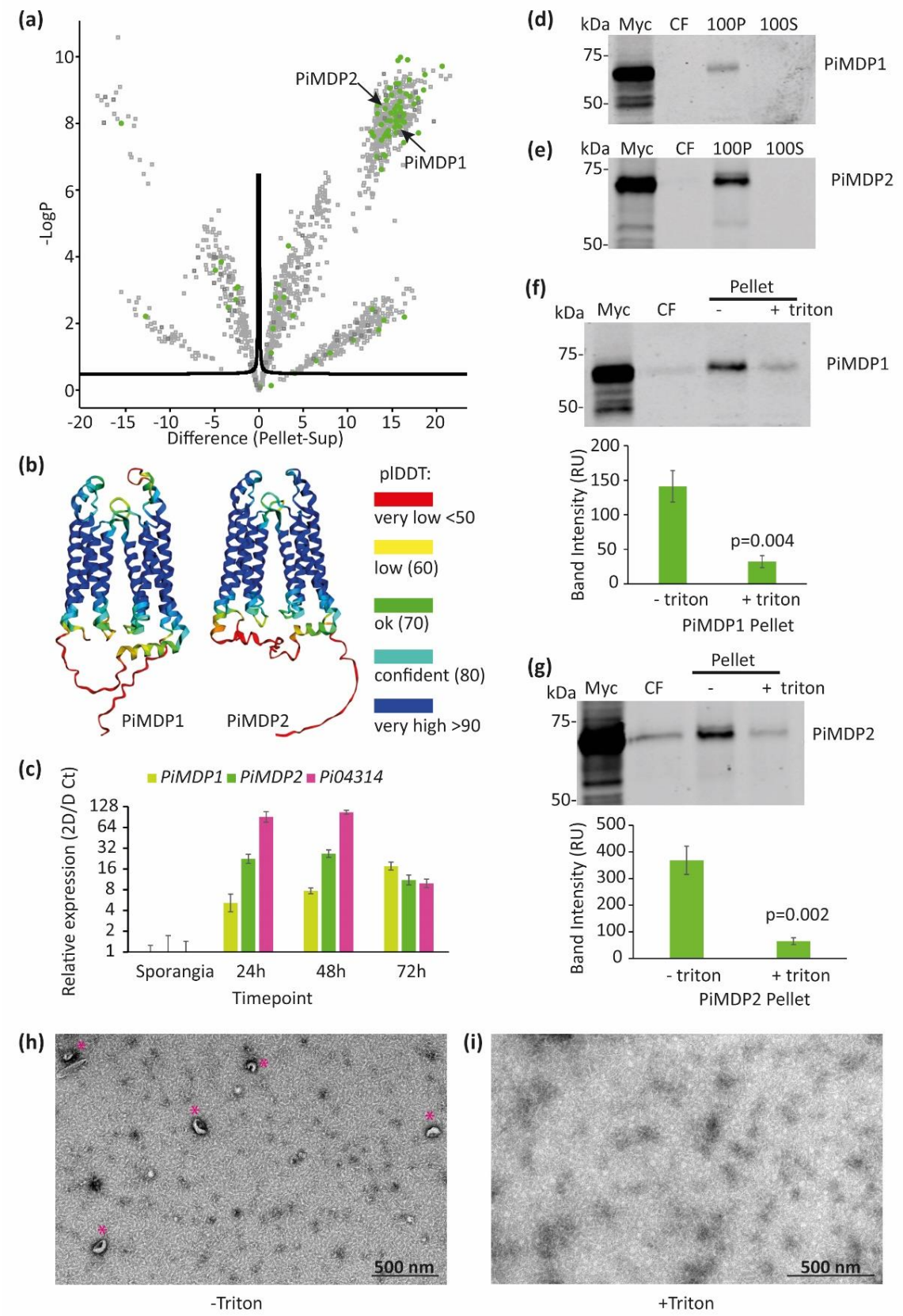

Figure 3: MARVEL-domain containing proteins are found exclusively in the crude vesicle pellet sample and are expressed during *P. infestans* infection. (a) Volcano plot showing the statistical distribution of proteins within the pellet vs supernatant samples. Green spots represent transmembrane (TM) domain containing proteins. Black arrows indicate the location of PiMDP1 and

904 PiMDP2. TM domains were identified using DeepTMHMM (https://dtu.biolib.com/DeepTMHMM). (b)
905 Predicted structures of PiMDP1 and PiMDP2 produced using Alphafold2. Protein structures are colour-
906 coded to show plDDT confidence levels as shown in the key. (c) Gene expression of PiMDP1, PiMDP2
907 and the RxLR Pi04314 over a time-course of *P. infestans* isolate 3928A infecting Maris Piper potato
908 leaves. Expression was normalised to the geometric mean of 3 housekeeping genes (ACTIN, Caesin
909 kinase, Kelch domain repeat) using the 2D/D Ct method. Error bars show St Error. (d-e) crude vesicle
910 pellet and supernatant isolation from transgenic *P. infestans* isolates expressing (d) PiMDP1-mCitrine
911 tagged protein, (e) PiMDP2-mCitrine tagged protein. These western blots show mycelia (M) and
912 culture filtrate (CF) samples prior to any centrifugation, 100,000 x*g* pellet (100P) and supernatant
913 samples after 100,000 x*g* spin (100S). These western blots confirm the localisation of the proteins
914 based on the observations from the volcano plot in (a). (f) -/+ 1% Triton treatment of culture filtrate
915 from PiMDP1-mCitrine expressing *P. infestans* isolate. This western blot shows mycelia (M) and culture
916 filtrate (CF) samples prior to any centrifugation and 100,000 x *g* pellet (100P) -/+ 1% Triton X-100. The
917 band intensity graph shows the relative intensity of 100P -/+ 1% Triton bands from 6 independent
918 replicates. Statistical analysis was done using a Paired T-test on SigmaPlot giving the two-tailed P value
919 of 0.004. (g) -/+ 1% Triton treatment of culture filtrate from PiMDP2-mCitrine expressing *P. infestans*
920 isolate. The western blot shows mycelia (M) and culture filtrate (CF) samples prior to any centrifugation
921 and 100,000 x*g* pellet (100P) -/+ 1% Triton. The band intensity graph shows the relative intensity of
922 100P -/+ 1% Triton bands from 5 independent replicates. Statistical analysis was done using a Paired T-
923 test on SigmaPlot giving the two-tailed P value of 0.002. (h) Transmission electron microscopy negative
924 stain image showing vesicles present within a – Triton sample from a transgenic *P. infestans* isolate
925 expressing both PiMDP1-mCitrine and Pi04314-mCherry. Asterisks indicate vesicles, scale bar
926 represents 500 nm. (i) Transmission electron microscopy negative stain image indicating the loss of
927 vesicles in an equivalent + Triton sample. Scale bar represents 500 nm.

928

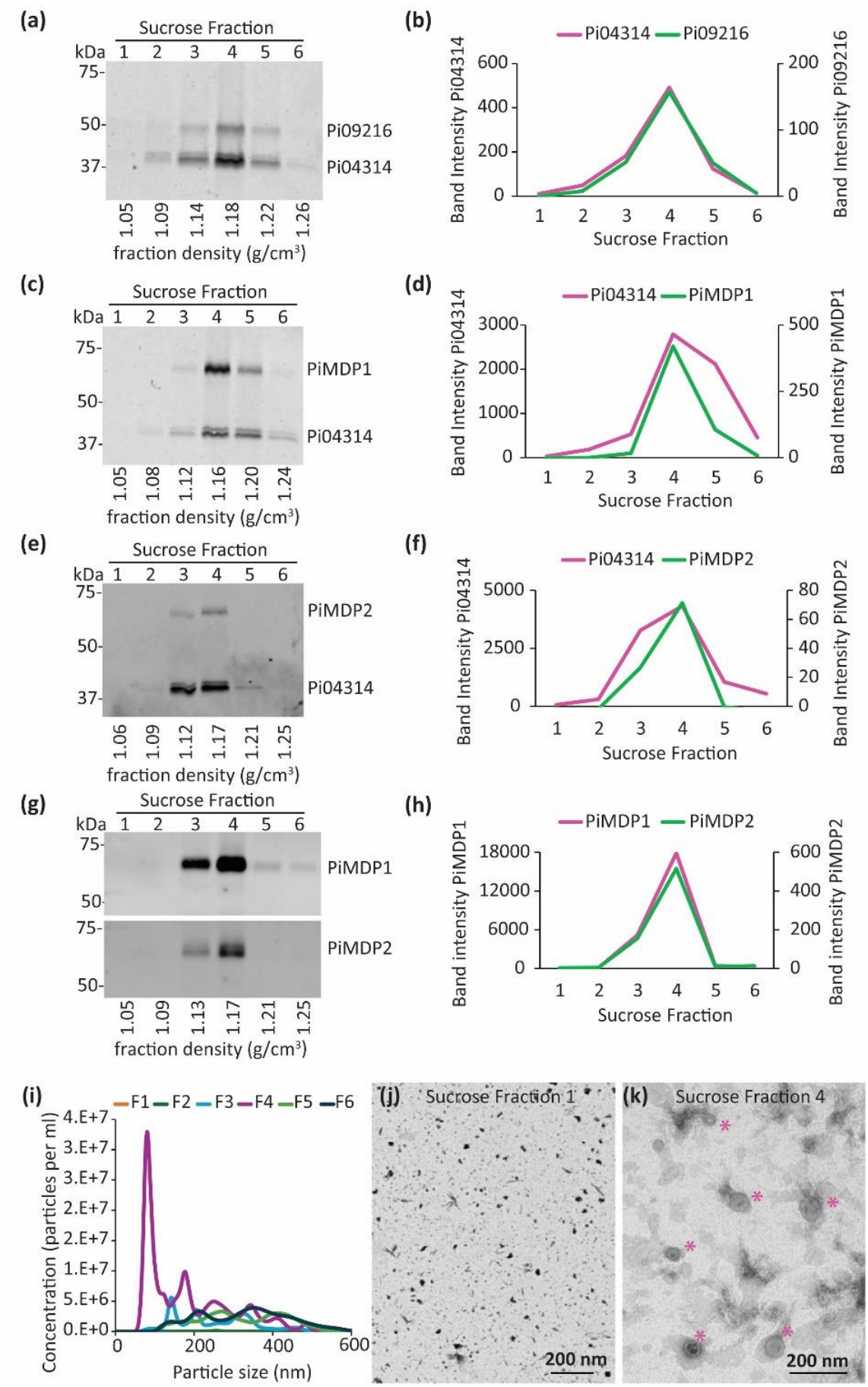
(a)
Sucrose Fraction
kDa 1 2 3 4 5 6
75-
50-
37-
Pi09216
Pi04314
1.05 1.09 1.14 1.18 1.22 1.26
fraction density (g/cm³)
(b)
Pi04314 Pi09216
Band Intensity Pi04314
Band Intensity Pi09216
Sucrose Fraction
(c)
Sucrose Fraction
kDa 1 2 3 4 5 6
75-
50-
37-
PiMDP1
Pi04314
1.05 1.08 1.12 1.16 1.20 1.24
fraction density (g/cm³)
(d)
Pi04314 PiMDP1
Band Intensity Pi04314
Band Intensity PiMDP1
Sucrose Fraction
(e)
Sucrose Fraction
kDa 1 2 3 4 5 6
75-
50-
37-
PiMDP2
Pi04314
1.06 1.09 1.12 1.17 1.21 1.25
fraction density (g/cm³)
(f)
Pi04314 PiMDP2
Band Intensity Pi04314
Band Intensity PiMDP2
Sucrose Fraction
(g)
Sucrose Fraction
kDa 1 2 3 4 5 6
75-
50-
PiMDP1
PiMDP2
1.05 1.09 1.13 1.17 1.21 1.25
fraction density (g/cm³)
(h)
PiMDP1 PiMDP2
Band intensity PiMDP1
Band intensity PiMDP2
Sucrose Fraction
(i)
F1 F2 F3 F4 F5 F6
Concentration (particles per ml)
Particle size (nm)
(j) Sucrose Fraction 1
200 nm
(k) Sucrose Fraction 4
200 nm

929

930 **Figure 4: MARVEL-domain and RxLR effector proteins are detected within the same sucrose density**
931 **fraction.** Crude vesicle pellets were top-loaded onto a discontinuous sucrose gradient consisting of 10,
932 20, 30, 40, 50, 60 and 70% layers. After centrifugation at 100K x*g* for 16 h, six fractions of 1.9 ml each
933 were collected and processed with further ultracentrifugation to obtain a pure vesicle pellet. All
934 membranes were dual probed with αGFP and αRFP. The density (g/cm^3) of each fraction is detailed
935 under each blot. (a) Six fractions isolated using a top-loaded crude pellet from a P. infestans isolate
936 expressing both Pi09216-mCitrine and Pi04314-mCherry. (b) Graph showing band intensity for
937 Pi09216-mCitrine (green) and Pi04314-mCherry (pink) from each fraction shown in (a) (c) Fractions
938 isolated from *P. infestans* expressing both PiMDP1-mCitrine and Pi04314-mCherry. (d) Graph showing
939 band intensity for PiMDP1-mCitrine (green) and Pi04314-mCherry (pink) from each fraction shown in
940 (c). (e) Fractions isolated from *P. infestans* expressing both PiMDP2-mCitrine and Pi04314-mCherry. (f)
941 Graph showing band intensity for PiMDP2-mCitrine (green) and Pi04314-mCherry (pink) from each
942 fraction shown in (e). (g) Fractions isolated from *P. infestans* expressing both PiMDP2-mCitrine and
943 mCherry-PiMDP1. (h) Graph showing band intensity for PiMDP2-mCitrine (green) and mCherry-
944 PiMDP1 (pink) from each fraction shown in (g). (i) Nanoparticle tracking (NTA) data showing the
945 number and size distribution of particles in each sucrose fraction. Results show the average from three
946 independent replicates for each sample. (j) Transmission electron microscopy negative stain image of
947 a sample of fraction 1 isolated from *P. infestans* isolate expressing both PiMDP1-mCitrine and Pi04314-
948 mCherry. (k) Transmission electron microscopy negative stain image showing a range of vesicles in
949 fraction 4 isolated from the same isolate. Asterisks indicate EV's, scale bars in I and j represent 200 nm.

950

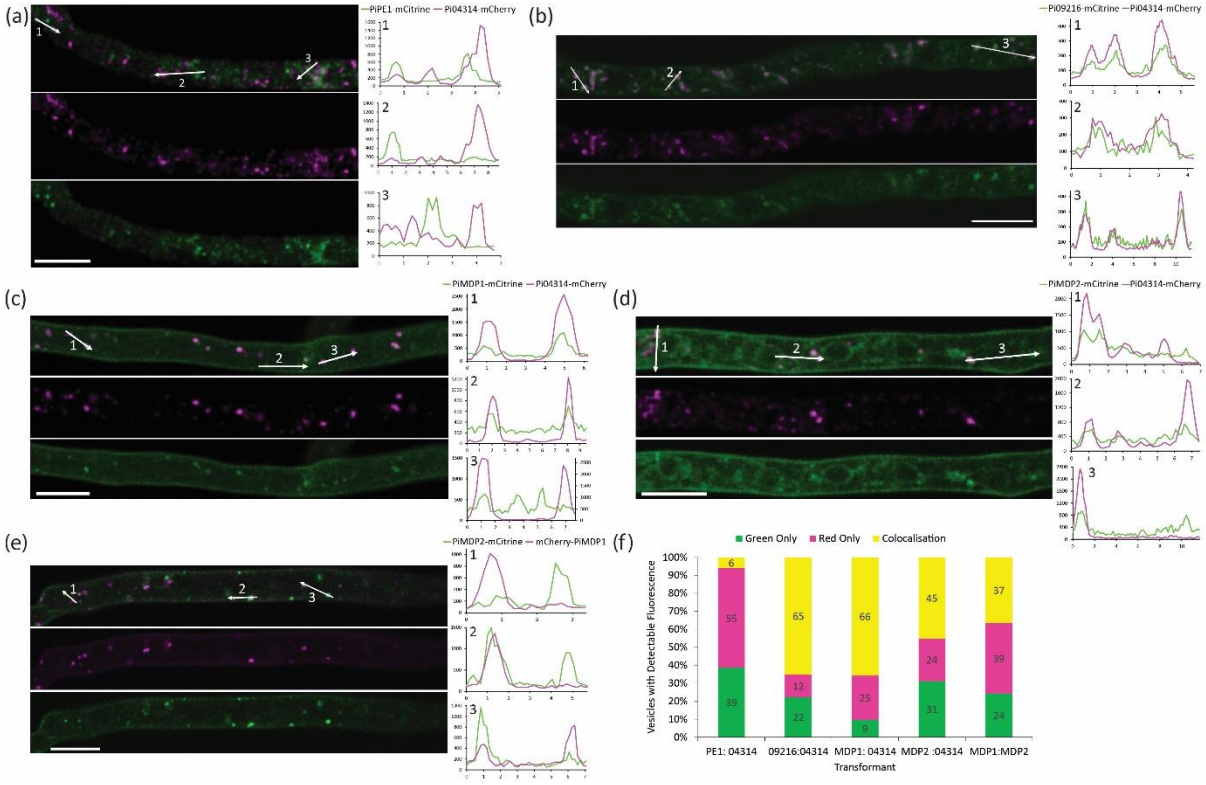

Figure 5: PiMDP1/PiMDP2 and RxLR proteins colocalise in vesicle-like structures in hyphae grown *in vitro*. Projection images from confocal z series images of hyphae from transformed *P. infestans* transgenic lines expressing fluorescent protein fusions grown on microscope slides. The mCitrine (green) and mCherry (magenta) channels are shown separately and merged with three numbered arrows indicating transects drawn using single optical sections to produce the three numbered fluorescence intensity plots to the right. The transgenic lines were co-expressing: (a) apoplastic effector PiPE1-mCitrine and RxLR Pi04314-mCherry; (b) RxLRs Pi09216-mCitrine and Pi04314-mCherry; (c) PiMDP1-mCitrine which localises to the PM and also partially co-localises to vesicles with Pi04314-mCherry; (d) PiMDP2-mCitrine which localises to the PM and also partially co-localises to vesicles with Pi04314-mCherry; (e) PiMDP2-mCitrine which partially co-localises to vesicles with mCherry-PiMDP1; both are observed at the PM. Scale bars are 10 µm. Fluorescence intensity plots show relative fluorescence on the y axis against distance in µm on the x axis. (f) Stacked bar chart shows quantification of the percentage of vesicles showing mCitrine only, mCherry only or colocalisation of both fluorophores. Results are the average counts from at least 12 images; percentages are shown on the chart; n indicates the total number of vesicles counted for each transformant (PiPE1-mCitrine & Pi04314-mCherry n= 612; Pi09216-mCitrine & Pi04314-mCherry n= 350; PiMDP1-mCitrine & Pi04314-mCherry n= 237; PiMDP2-mCitrine & Pi04314-mCherry n= 303; PiMDP2-mCitrine & mCherry-PiMDP1 n= 293).

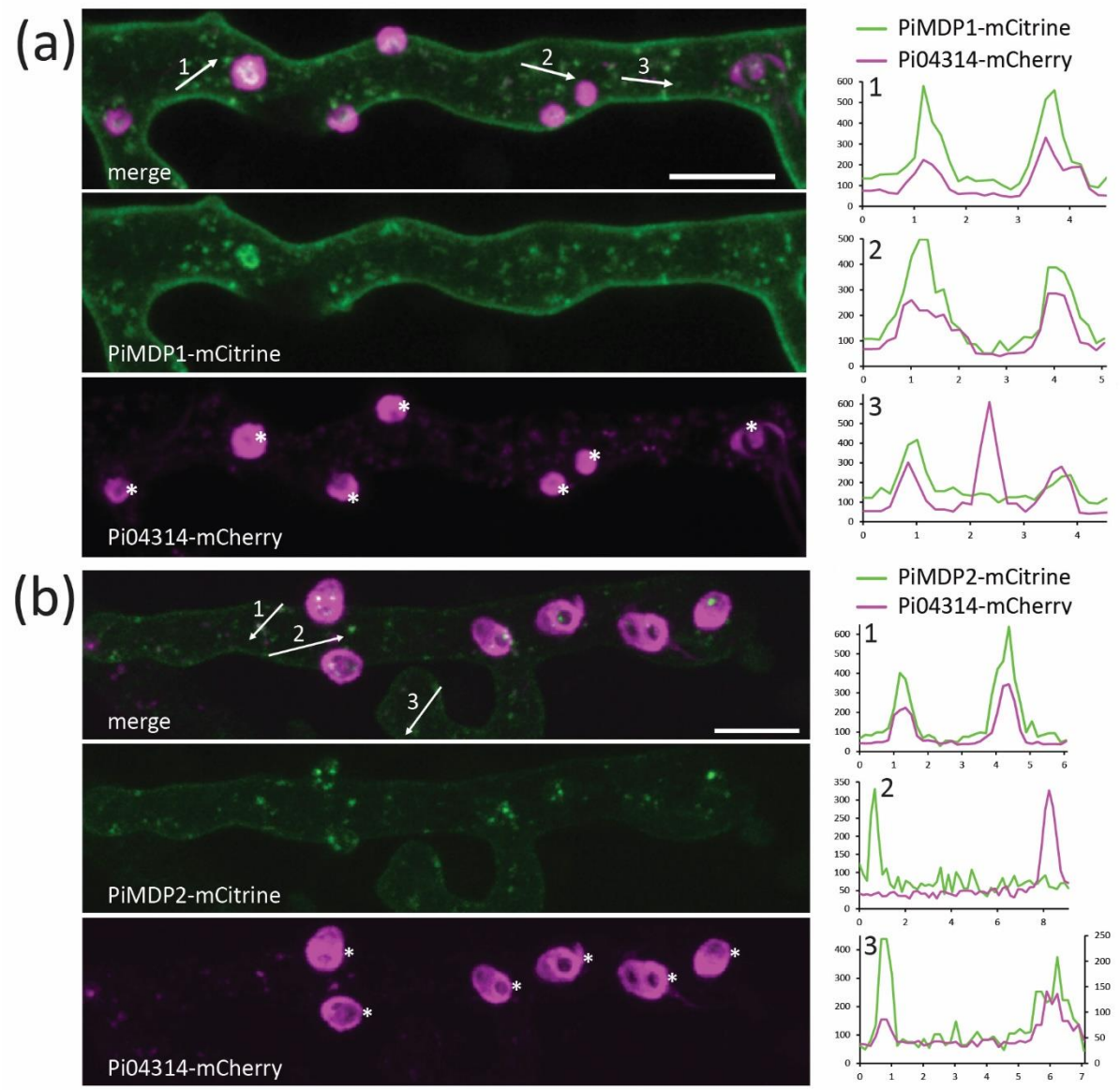

Figure 6: PiMDP and RxLR proteins co-localise in vesicle-like structures in hyphae during infection.

Projection images from confocal z series of hyphae from transformed *P. infestans* isolates expressing fluorescent protein fusions infecting *N. benthamiana* leaves. The mCitrine (green) and mCherry (pink) channels are shown separately and merged with three numbered arrows indicating transects drawn using single optical sections to produce the three numbered fluorescence intensity plots below. (a) PiMDP1-mCitrine localises to the plasma membrane (PM) and partially co-localises to vesicles with Pi04314-mCherry. (b) PiMDP2-mCitrine localises to the PM and partially co-localises to vesicles with Pi04314-mCherry. The mCherry intensities were low in this hypha and thus are plotted with the right-hand vertical axis to make the patterns more obvious. Asterisks indicate haustoria and scale bars are 10 µm. Fluorescence intensity plots show relative fluorescence on the y axis against distance in µm on the x axis.

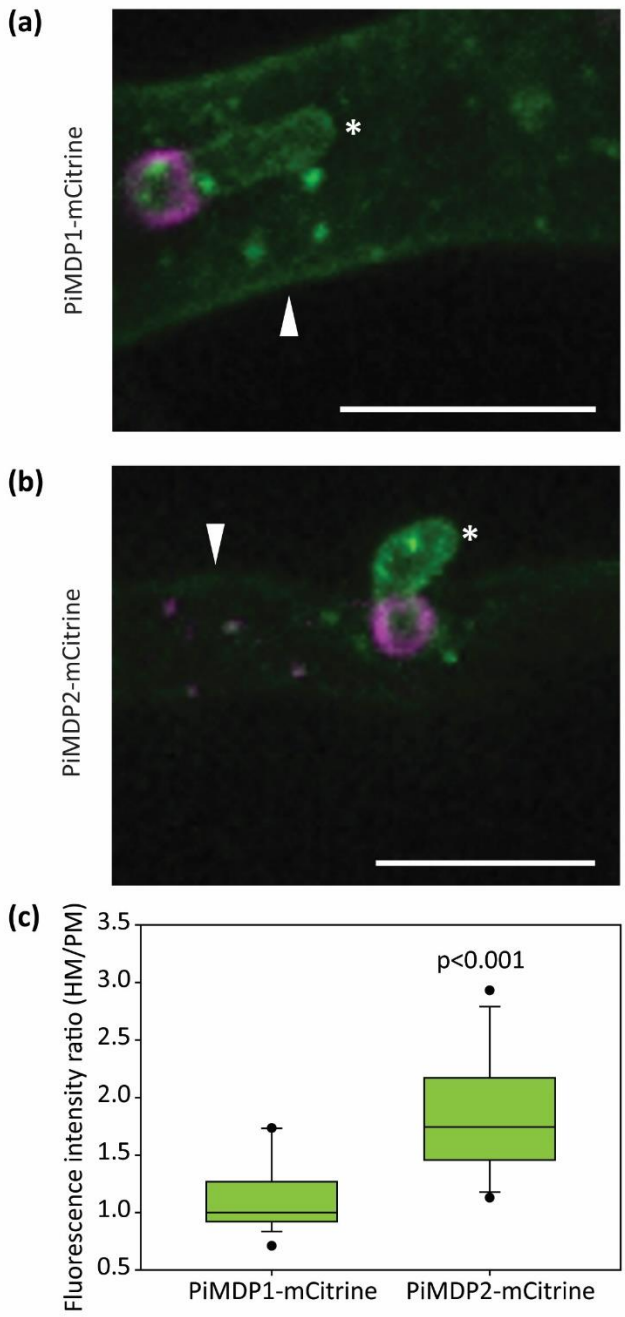

Figure 7: PiMDP2-mCitrine accumulates in the mature haustorial membrane during infection. Confocal projection images from z series images of *P. infestans* hyphae and haustoria during plant infection showing (a) PiMDP1-mCitrine localised to the plasma membrane (PM), haustorial membrane (HM) and vesicle-like bodies in the hypha, with 04314-mCherry localised around the haustoria and, (b) PiMDP2-mCitrine accumulates more strongly in the HM with little PM fluorescence, in addition to vesicle-like bodies in the hypha, with 04314-mCherry localised around the haustoria. Asterisks indicate haustoria, arrowheads indicate the PM and the scale bars are 10 μM. (c) Boxplot shows quantification of the ratio of the relative fluorescence intensity in regions of the HM compared to the PM measured from single optical sections. The points indicate the 5th and 95th percentile outliers and the lines show the median values. Statistical analysis was done using a Mann-Whitney Rank Sum Test on SigmaPlot giving the P value of <0.001, (n≥ 19).